ApJ, in press: 22 September 2002

Our Sun. IV. The Standard Model and Helioseismology: Consequences of Uncertainties in Input Physics and in Observed Solar Parameters

Arnold I. Boothroyd[1] and I.-Juliana Sackmann[2]

W. K. Kellogg Radiation Laboratory 106-38, California Institute of Technology, Pasadena, CA 91125

boothroy@cita.utoronto.ca

ijs@caltech.edu

ABSTRACT

Helioseismology provides a powerful tool to explore the deep interior of the Sun. Measurements of solar interior quantities are provided with unprecedented accuracy: for example, the adiabatic sound speed c can be inferred with an accuracy of a few parts in 10^4. This has become a serious challenge to theoretical models of the Sun. Therefore, we have undertaken a self-consistent, systematic study of sources of uncertainties in the standard solar model, which must be understood before the helioseismic observations can be used as constraints on the theory. This paper focusses on our own current calculations, but is also a review paper summarizing the latest calculations of other authors. We find that the largest uncertainty in the sound speed c in the solar interior, namely, 3 parts in 10^3, arises from uncertainties in the observed photospheric abundances of the elements: C, N, O, and Ne have uncertainties of $\sim 15\%$, leading to an uncertainty of $\sim 10\%$ in the photospheric Z/X ratio. Uncertainties of 1 part in 10^3 in the sound speed c arise, in each case, from (1) the $\sim 4\%$ uncertainty in the OPAL opacities, (2) the $\sim 5\%$ uncertainty in the basic *pp* nuclear reaction rate, (3) the $\sim 15\%$ uncertainty in the diffusion constants for the gravitational settling of helium, and (4) the $\sim 50\%$ uncertainties in diffusion constants for the heavier elements. (Other investigators have shown that similar uncertainties arise from uncertainties in the interior equation of state and in rotation-induced turbulent mixing.) In the convective envelope *only*, uncertainties in c of order 1 part in 10^3 arise from the uncertainty of a few parts in 10^4 in the solar radius, and from uncertainties in the low-temperature equation of state. Other current uncertainties, namely, in the solar age and luminosity, in nuclear rates other than the *pp* reaction, and in the low-temperature molecular opacities, have no significant effect on the quantities that can be inferred from helioseismic observations. Significant uncertainty in the convective envelope position R_{ce} (of up to 3 times the observational uncertainty of $\pm 0.001\ R_\odot$) arises only from uncertainties in Z/X, opacities, the *pp* rate, and helium diffusion constants; the envelope helium abundance Y_e is significantly affected (± 0.005) only by extreme variations in Z/X, opacities, or diffusion constants, and is always consistent with the "observed" range of helioseismically inferred Y_e values. Our predicted pre-main-sequence solar lithium depletion is a

[1]Present address: CITA, U. of Toronto, 60 St. George Street, Toronto, Ontario, Canada M5S 3H8

[2]Present address: West Bridge Laboratory 103-33, California Institute of Technology, Pasadena, CA 91125

factor of ~ 20 (an order of magnitude larger than that predicted by earlier models that neglected gravitational settling and used older opacities), and is uncertain by a factor of 2. The predicted neutrino capture rate is uncertain by $\sim 30\%$ for the ^{37}Cl experiment and by $\sim 3\%$ for the ^{71}Ga experiments (not including uncertainties in the capture cross sections), while the ^{8}B neutrino flux is uncertain by $\sim 30\%$.

Subject headings: diffusion — neutrinos — Sun: abundances — Sun: helioseismology — Sun: interior

1. Introduction

Helioseismology provides a powerful tool to explore the deep interior of the Sun. Measurements of solar interior quantities are provided with unprecedented accuracy. The Michelson Doppler Imager (MDI) on the Solar and Heliospheric Observatory (SOHO) spacecraft (Rhodes et al. 1997), the Global Oscillation Network Group (GONG: see, e.g., Gough et al. 1996; Harvey et al. 1996), the Birmingham Solar Oscillation Network (BiSON: Chaplin et al. 1996), and the Low-l instrument (LOWL: Tomczyk et al. 1995) provide helioseismic frequency measurements with accuracies of a few parts in 10^5. From these, the sound speed c throughout most of the solar interior can be inferred with an accuracy of a few parts in 10^4, as can the adiabatic index Γ_1; the density can be inferred with an accuracy of a few parts in 10^3 (Basu, Pinsonneault, & Bahcall 2000; Bahcall, Pinsonneault, & Basu 2001). The depth of the solar envelope convection can be measured with an accuracy of nearly a part in 10^3 (Basu & Antia 1997). The abundance of helium in the solar envelope can also be inferred, but this value depends on the solar equation of state (see, e.g., Basu & Antia 1995; Richard et al. 1998; Di Mauro et al. 2002); as discussed in § 3.3, this inferred helium abundance appears to be uncertain at the level of a few percent (i.e., an uncertainty of at least 0.005 in the helium mass fraction Y_e).

The ultimate goal of our work was to explore systematically a wide range of solar models with relatively modest amounts of mass loss on the early main sequence, and to test their viability via helioseismological measurements (as well other observational constraints). This mass loss investigation is presented in our companion paper "Our Sun V" (Sackmann & Boothroyd 2002). Since the consequences of moderate early solar mass loss are expected to be small, it is essential to understand the consequences of uncertainties in the input physics and in the input parameters of the solar model. The physics inputs include the equation of state, opacities, nuclear rates, diffusion constants, the treatment of convection (including the possibility of overshoot), and the effects of rotation and mass loss. Observed solar parameters include the solar age and the present solar radius, luminosity, surface composition, and solar wind. A considerable amount of work has been published investigating many of the above effects, as will be discussed in § 3. However, some basic uncertainties still warrant further attention. Before proceeding to our mass loss work, we found it necessary to try to extend the investigations of the above uncertainties. In particular, the major consequences arising from uncertainties in the present observed solar surface Z/X ratio, in the basic p-p chain rate, and in the diffusion constants for gravitational settling of helium and the heavy elements, have not been addressed sufficiently in the recent (most accurate) work of other investigators. To determine the consequences of these uncertainties, we computed standard solar models with various values of the Z/X ratio, the p-p chain rate, and the diffusion constants (lying in the permitted ranges). To obtain a set of self-consistent results, we also investigated the consequences of a number of other uncertainties, namely, in other nuclear rates, in envelope opacities, in the equation of state, from different methods of handling interior opacities, and in the solar age, luminosity, and radius. It is the aim of this paper to present the effects of the above uncertainties on the run of the sound speed and density in the solar interior, and on the radius R_{ce} of solar convection

and the solar envelope helium abundance Y_e. We also present the effects on the pre-main-sequence solar lithium depletion (excluding rotation effects) and on the production of solar neutrinos. (Note that lithium depletion in a non-rotating standard solar model occurs entirely on the pre-main-sequence; this predicted depletion is significantly smaller than the observed solar lithium depletion factor. Rotational mixing on the main sequence is generally invoked to account for the remaining lithium depletion).

2. Methods

We computed a reference standard solar model using up-to-date physics plus the observed values for the solar parameters. Several dozen variant solar models were also computed, in which one of these "inputs" was varied within the allowed uncertainties. (In a few cases, more than one of the "inputs" was varied, or the size of the variation exceeded the size of the quoted uncertainty in order to get a better estimate of the sensitivity.) By comparing with the reference standard solar model, the sensitivity to the uncertainties in the "inputs" could be determined. The stellar evolution code used to compute these solar models is descended from that used earlier in our "Sun III" paper (Sackmann, Boothroyd, & Kraemer 1993; see also Boothroyd & Sackmann 1999), but has been extensively updated for improved accuracy, including provision for much finer zoning as well as up-to-date input physics.

Equation of State: The reference standard solar model used the OPAL equation of state (Rogers, Swenson, & Iglesias 1996) in the interior, and the MHD equation of state (Däppen et al. 1988) where it was designed to be accurate, namely, in the outer envelope at $\log \rho \lesssim -2$ (this corresponds to $r \gtrsim 0.94\ R_\odot$ and $\log T \lesssim 5.5$ in the present Sun). A version of the MHD equation of state computation program was kindly provided to us (D. Mihalas 1999, private communication), and minor modifications allowed computation of the MHD equation of state for various hydrogen abundances and metallicities down to pre-main-sequence photospheric temperatures and even below (A. I. Boothroyd, in preparation). In both cases, the equation of state was interpolated in metallicity Z as well as in hydrogen abundance X, temperature T, and density ρ, in order to take into account metallicity variations due to diffusion and nuclear burning. Tables for the MHD equation of state were computed on the same $\{X, Z, T, \rho\}$ grid as the OPAL tables, with the following exceptions: for MHD, the upper ρ limit was slightly higher than for OPAL at low temperatures, but lower at high temperatures (since it never exceeded $\log \rho = -1.5$); below $log T = 3.7$, intervals of $\Delta \log T = 0.01$ were used for the MHD T-grid, the same as the average $\log T$ interval in the OPAL grid for $0.005 \leq T_6 \leq 0.006$ ($3.7 \lesssim \log T \lesssim 3.78$); and for $0.006 \leq T_6 \leq 0.05$ ($3.78 \lesssim \log T \lesssim 4.7$), extra T-grid points were added to double the density of the grid as a function of temperature in this region. By computing some MHD tables at intermediate grid-values, the interpolation accuracy in each of $\{X, Z, T, \rho\}$ was tested. In the outer solar convective zone ($r \gtrsim 0.95\ R_\odot$), the fractional error in the pressure P was $\lesssim 2 \times 10^{-4}$, and for derivative quantities such as C_v, χ_T, χ_ρ, and Γ_1, the fractional error was $\lesssim 2 \times 10^{-3}$; deeper in the Sun ($r < 0.95\ R_\odot$), the interpolation errors were nearly an order of magnitude smaller. The interpolation accuracy is thus several times better than the quoted precision of the OPAL equation of state in the corresponding regions (Rogers et al. 1996).

Variant cases were tested where the OPAL equation of state was used down to $\log T = 4$ or even all the way down to its lower limit of validity at $\log T = 3.7$ — in the latter case, the MHD equation of state was relevant only to the pre-main-sequence evolution. The MHD equation of state tables computed for this work considered H and He, plus a 13-element subset of the Grevesse & Noels (1993) heavy element composition (i.e., C, N, O, Ne, Na, Mg, Al, Si, S, Ar, K, Ca, and Fe); besides the effects due to neutrals and ions, effects

due to H^-, H_2, and H_2^+ were accurately taken into account, and approximate effects of the molecules C_2, N_2, O_2, CH, CN, CO, NH, NO, OH, CO_2, and H_2O (although these molecules have no effect for solar models: they were actually added in anticipation of use in asymptotic giant branch models). The OPAL equation of state considers only H, He, C, N, O, and Ne (plus hydrogen-molecule effects); however, the equation of state is quite insensitive to the precise makeup of the metallicity, and the OPAL equation of state may well be the more accurate one in the region where both are valid (Rogers et al. 1996; Gong, Däppen, & Nayfonov 2001a).

It has been noted that patching together equations of state can introduce spurious effects (Däppen et al. 1993; Basu, Däppen, & Nayfonov 1999). Such spurious effects were minimized in the present work by (1) performing a gradual switchover over a finite density or temperature region, to avoid any discontinuities, and (2) choosing switchover regions where the two equations of state were quite similar. The three switchover regions comprised $-1.5 > \log \rho > -2$ (corresponding to $5.8 > \log T > 5.5$ in the present Sun), $4.0 > \log T > 3.9$, or $3.75 > \log T > 3.7$; in the first and last of these regions, the MHD and OPAL equations of state under solar conditions differ typically by several parts in 10^3 (with differences in the pressure P being several times smaller than this), i.e., only a few times worse than the expected precision of the equations of state. Near $\log T = 4$, the differences were nearly an order of magnitude smaller (and also remained small over a very wide range of densities). Any spurious effects from the switchover should be smaller than spurious effects arising from the fact that the OPAL equation of state is not self-consistent, with the size of the inconsistency (in the outer Solar envelope) being comparable to the size of the differences between the OPAL and MHD equations of state (as discussed in § 3.1).

Opacities: For interior temperatures ($\log T > 4$), our reference standard solar model used the 1995 OPAL opacities (Iglesias & Rogers 1996) — these opacities use the Grevesse & Noels (1993) "GN93" solar composition, and we refer to these opacities as "$\kappa_{\rm OPAL:GN93}$." The online opacity computation feature of the OPAL web page[3] allowed computation of OPAL opacities appropriate to the more recent Grevesse & Sauval (1998) "GS98" mixture ("$\kappa_{\rm OPAL:GS98}$"); these were tested in variant models, as were opacities appropriate to the older Grevesse (1984) "Gr84" mixture ("$\kappa_{\rm OPAL:Gr84}$"). The even older and much less accurate Los Alamos (LAOL) opacities "$\kappa_{\rm LAOL85}$" (Keady 1985, private communication) were also tested in one case. At cool envelope temperatures ($\log T \lesssim 4$), our reference standard solar model used the Alexander & Ferguson (1994) opacities "$\kappa_{\rm Alexander}$" (which include molecular opacities). We also tested the effect of using the Sharp (1992) molecular opacities "$\kappa_{\rm Sharp}$" at cool envelope temperatures instead.

In our reference standard solar model, we did our best to account for temporal and spatial variations in the opacity due to composition changes from diffusion and nuclear burning. The OPAL opacity tables allow interpolation of the opacity as a function of the hydrogen abundance and the metallicity Z; the abundances of the metals comprising Z are always proportional to Z in the OPAL tables, i.e., a "scaled solar" distribution. In addition, the OPAL opacity tables contain mixtures with excess carbon and oxygen (beyond that contained in the scaled solar metallicity), allowing interpolation in carbon and oxygen abundances.

To take into account the variations in abundance due to diffusion, the metallicity value Z_κ that we used for metallicity interpolation in the OPAL opacity tables was proportional to the abundances of the elements heavier than oxygen: $Z_\kappa = Z_h$, where $Z_h \equiv Z_0[\sum_{heavy} X_i]/[\sum_{heavy}(X_i)_0]$, where Z_0 and $(X_i)_0$ are the protosolar metallicity and composition, respectively, and $\sum_{heavy}$ refers to a sum over elements heavier

[3]http://www-phys.llnl.gov/Research/OPAL/

than oxygen. In other words, we scaled the initial solar metallicity by the shift in heavy element abundances resulting from diffusion (note that our diffusion routines assumed that all metals diffused alike). However, for the CNO elements, there are additional changes due to nuclear burning, so that the CNO abundance profiles are not proportional to the heavy element abundance profiles; Turcotte et al. (1998) find that conversion of C and O into N results in an opacity change of $\sim 1\%$ that cannot be modelled by a change in Z alone. These variations in the CNO elements relative to Z_h were accounted for in an approximate manner by an additional two-dimensional interpolation in nominal "excess carbon and oxygen" abundances C_{ex} and O_{ex}, where these excess abundances account for any variation in the CNO abundances relative to the scaled solar metallicity Z_κ of the OPAL opacity tables. Since there were no explicit opacity tables for changes in nitrogen, the best one could do was to distribute excess nitrogen equally between C_{ex} and O_{ex} (i.e., to assume that nitrogen opacities were midway between those of carbon and oxygen): $C_{ex} = C - C_0\, Z_\kappa/Z_0 + 0.5(N - N_0\, Z_\kappa/Z_0)$ and $O_{ex} = O - O_0\, Z_\kappa/Z_0 + 0.5(N - N_0\, Z_\kappa/Z_0)$, such that $CO_{ex} \equiv C_{ex} + O_{ex} = Z - Z_\kappa$.

Note that in general, as first carbon and then oxygen is burned to nitrogen, either C_{ex} or O_{ex} will be negative, implying *extrapolation* of the OPAL tables in the direction of zero C or O by a non-negligible fraction of Z. One might consider the uncertainties in such an extrapolation to be worse than the error inherent in treating all CNO opacities alike; in this case, if one of C_{ex} or O_{ex} was negative, one would set it to zero and subtract an equivalent amount from the other (so that the sum $C_{ex} + O_{ex}$ remains unchanged) — this was the method followed in our reference models. However, we also tested the case where negative values were allowed, extrapolating as required. These turned out to yield essentially identical results to the reference model: the rms difference was only 0.00006 in the sound speed profile $\Delta c/c$ and 0.0003 in $\Delta\rho/\rho$, comparable to the estimated numerical accuracy of the models. An alternative case where this latter CNO variation was not approximated by excess CO at all, i.e., having $Z_\kappa = Z_h$ but $CO_{ex} = 0.0$, also yielded almost identical results (rms difference of 0.00005 in $\Delta c/c$ and 0.0004 in $\Delta\rho/\rho$). Similarly negligible rms differences were found for several cases testing different prescriptions for defining Z_h, C_{ex}, and O_{ex} (differing in whether mass fractions or number densities were used, in how the excess nitrogen was divided between C_{ex} and O_{ex}, and in whether negative values were allowed for C_{ex} and O_{ex}).

Finally, one run was computed where CNO-interpolation in the opacities was actually performed. In addition to the standard OPAL opacity table, the OPAL web page[4] was used to compute an opacity table with a composition where C had been converted to N, and one where both C and O had been converted to N; the model CNO abundances were used to interpolate in opacity among these tables. This "CNO-interpolation" model also yielded results essentially identical to the reference model (an rms difference of 0.00006 in $\Delta c/c$ and 0.0005 in $\Delta\rho/\rho$).

An estimate for the upper limit of the effects of opacity uncertainties was made by simply setting $Z_\kappa = f\, Z$ for a constant factor $f = 0.9$, 0.95, 1.0, 1.05, or 1.10; note that the case $f = 1.0$ is only slightly different from the reference standard solar model.

Nuclear Reaction Rates: The reference standard solar model used the NACRE nuclear reaction rates (Angulo et al. 1999), supplemented by the ^{7}Be electron capture rates of Gruzinov & Bahcall (1997) for $\log T \geq 6$ and of Bahcall & Moeller (1969) for $\log T < 6$ (note that this latter low-temperature region is irrelevant for solar models). Variant models tested cases with nuclear rates changed according to the upper or lower limits quoted in the NACRE compilation; one case tested the use of the older Caughlan & Fowler

[4]http://www-phys.llnl.gov/Research/OPAL/type1inp.html

(1988) nuclear rates. The program uses the minimum of the weak (Salpeter 1955), intermediate (Graboske et al. 1973), or strong (Itoh et al. 1979; Ichimaru & Utsumi 1983) screening factors (note that both weak and intermediate screening formulae include a term to take partial electron degeneracy into account) — for solar conditions, this choice leads to the use of weak screening, which is a very good approximation to the exact quantum mechanical solution there (see, e.g., Bahcall, Chen, & Kamionkowski 1998b; Gruzinov & Bahcall 1998). Deuterium was not considered separately (it was assumed to have been entirely burned to ^{3}He on the early pre-main-sequence), but all the other 15 stable isotopes up to and including ^{18}O were considered in detail (i.e., nuclear equilibrium was not assumed for any of them). The other stable isotopes up to ^{28}Si were included in the code (plus a few long-lived unstable isotopes, as well as Fe and a category for the sum of the other elements heavier than Si), but their nuclear reactions were not included since there are no significant effects under solar conditions (except for ^{19}F, which was assumed to be in CNO-cycle nuclear equilibrium for nuclear rate purposes). Neutrino capture cross sections were taken from Bahcall & Ulrich (1988), except for the ^{8}B-neutrino cross section for capture on ^{37}Cl, where the more recent value (5% higher) of Aufderheide et al. (1994) was used.

Diffusion: A set of subroutines[5] were kindly provided to us (M. H. Pinsonneault 1999, private communication) that take into account the diffusion (gravitational settling) of helium and heavy elements relative to hydrogen (see also Thoul, Bahcall, & Loeb 1994; Bahcall, Pinsonneault, & Wasserburg 1995). These subroutines assume that all heavy elements diffuse at the same rate as fully-ionized Fe; this yields surprisingly accurate results, as may be seen by comparing to the results of a more detailed treatment (Turcotte & Christensen-Dalsgaard 1998; Turcotte et al. 1998). The upper limit of the effects of uncertainties in the diffusion constants was estimated by simply multiplying the diffusion constants, either for helium or for the heavy elements, by a constant factor.

Convection: The Schwarzschild criterion was used to define convective boundaries; no core overshooting or envelope undershooting was allowed. Note that Morel, Provost, & Berthomieu (1997) found that including convective core overshooting had a negligible effect on the solar sound speed and density profiles, but on the other hand that including convective envelope undershooting by even a tenth of a pressure scale height moved the solar convective envelope boundary inwards by eight times the uncertainty in the observed value, yielding a sharp spike in the difference between observed and calculated sound speed profiles. Rotation-induced mixing was not considered in our models; the effect that it would have is discussed in § 3.1.

Composition: The reference standard solar model used a value of $Z/X = 0.0245$ for the the present solar surface metals-to-hydrogen ratio (by mass fraction), as given by Grevesse & Noels (1993). Variant models tested the $\sim 13\%$ higher older value of $Z/X = 0.0277$ (Grevesse 1984; Anders & Grevesse 1989), as well as the 6% lower value of $Z/X = 0.023$ recommended as a "preliminary" value by the recent work of Grevesse & Sauval (1998). Values of $Z/X = 0.0203$ and 0.0257 were also used, for cases where the C, N, O, and Ne abundances of the Grevesse & Sauval (1998) mixture were all either decreased or increased, respectively, by their quoted uncertainties.

For a given solar model, the presolar abundances of the heavy elements were always taken from the OPAL opacity tables that we used for that solar model. For the reference standard solar model and most

[5]These subroutines are also available from Bahcall's web page: http://www.sns.ias.edu/~jnb/

variants, the "$\kappa_{\rm OPAL:GN93}$" opacities were used, which have the composition mix of Grevesse & Noels (1993). A variant model with a low value $Z/X = 0.023$ used instead the composition mix of Grevesse & Sauval (1998), and the corresponding "$\kappa_{\rm OPAL:GS98}$" opacities. Similarly, a variant model with a high value of $Z/X = 0.0277$ used of the abundance mix of Grevesse (1984), and the corresponding "$\kappa_{\rm OPAL:Gr84}$" opacities. Tests were also made with C, N, O, and Ne abundances increased or decreased by their uncertainties of 15% relative to Fe, with the OPAL opacities appropriate to these revised mixes: we refer to these as "$\kappa_{\rm OPAL:GN93\uparrow C-Ne}$" and "$\kappa_{\rm OPAL:GN93\downarrow C-Ne}$," respectively, when variations are relative to the Grevesse & Noels (1993) mix, and as "$\kappa_{\rm OPAL:GS98\uparrow C-Ne}$" and "$\kappa_{\rm OPAL:GS98\downarrow C-Ne}$" when variations are relative to the Grevesse & Sauval (1998) mix.

Solar Mass: A present solar mass of $M_\odot = 1.9891 \times 10^{33}$ g (Cohen & Taylor 1986) was used in all cases. Their quoted uncertainty of 0.02% is too small to have any significant effect, and is in fact smaller than the amount of mass lost by the Sun in the form of radiation ($\Delta M = \Delta E/c^2$ yields a mass loss of 0.03%, where ΔE is the total energy radiated away via photons and neutrinos since the Sun formed). Mass loss from the present solar wind is also small, and even if the average solar wind over the past 4.6 Gyr had been an order of magnitude higher than its present value, as is suggested by measurements of noble gas isotopes in lunar rocks (Geiss 1973; Geiss & Bochsler 1991; Kerridge et al. 1991), the total amount of mass lost would be about 0.2% (i.e., a total mass loss of $\leq 0.002\ M_\odot$ during the Sun's lifetime up to the present). Mass loss of this amount would yield negligible changes in the solar sound speed profile (about a part in 10^4), as shown in our companion paper "Our Sun V" (Sackmann & Boothroyd 2002). Solar mass loss was therefore ignored for all cases considered in this paper.

Note that, based on a correlation of X-ray flux with their measured mass loss rates in nine GK dwarfs, Wood et al. (2002) have recently proposed a mass loss time dependence $\dot{M} \propto t^{-2.00\pm0.52}$ in such stars (i.e., in main sequence stars with masses not too far from that of the Sun), with a maximum mass loss rate of $\sim 10^3$ times that of the present solar wind. This is discussed in our companion paper "Our Sun V" (Sackmann & Boothroyd 2002), and will be investigated in more detail in a future work (A. I. Boothroyd & I.-J. Sackmann, in preparation). In summary, total solar mass loss from the formula of Wood et al. (2002) could be of order 0.01 $M_\odot$, but most of this would take place very early on the main sequence due to the t^{-2} time dependence, so the effect should be relatively small, at most a few parts in 10^4 in the sound speed profile.

Solar Luminosity: For the reference standard solar model and most variant cases, a present solar luminosity of $L_\odot = 3.854 \times 10^{33}$ erg s^{-1} was used, as discussed in Sackmann et al. (1993). A value 0.3% lower (3.842×10^{33} erg s^{-1}) with an estimated 1-σ uncertainty of 0.4% was recently obtained by Bahcall et al. (2001), based on the observations of Fröhlich & Lean (1998) and Crommelynck et al. (1996). Variant models considered the effect of using this more recent solar luminosity value, and high and low values 2-σ (0.8%) above and below it. Note that most of the uncertainty in $L_\odot$ comes not from uncertainties in the present solar irradiance, but rather from uncertainties in the slight long-term variability of the solar luminosity. For example, Lean (2000) estimates a difference of 0.2% between the present value and that during the seventeenth century Maunder Minimum.

Solar Radius: The reference standard solar model used a solar radius at the photosphere ($\tau = 2/3$) of $R_\odot = 695.98$ Mm (Ulrich & Rhodes 1983; Guenther et al. 1992). Variant models considered the effect of

using the value of 695.78 Mm suggested by the helioseismic f-mode study of Antia (1998), or the value of 695.508 Mm suggested by the solar-meridian transit study of Brown & Christensen-Dalsgaard (1998).

Solar Age: In his Appendix to Bahcall et al. (1995), G. J. Wasserburg provides a systematic analysis of the upper and lower bounds on the age of the Sun, as obtained from isotopic ratios measured in meteorites. We briefly paraphrase his discussion in this paragraph: The protosolar nebula (out of which the Sun and the meteorites formed) contained not only the stable isotope ^{27}Al but also the unstable isotope ^{26}Al, which decays into ^{26}Mg with a half-life of only 0.7 Myr. This ^{26}Al must have been injected into the protosolar nebula from the stellar source where it was created. Isotopic measurements of meteoritic crystallized refractory condensates show that they had a ratio $^{26}\mathrm{Al}/^{27}\mathrm{Al} = 5 \times 10^{-5}$ at the time they formed. Even if the stellar source of the ^{26}Al had a very high ratio $^{26}\mathrm{Al}/^{27}\mathrm{Al} \sim 1$, the time interval between the formation of the ^{26}Al and the formation of the meteorite cannot have exceeded ~ 11 Myr (due to the short decay timescale of ^{26}Al). The Sun cannot have formed later than these meteorites. However, the Sun/meteorite system must have formed after the injection of ^{26}Al into the protosolar nebula, so the Sun cannot have formed earlier than ~ 11 Myr before the formation of these meteorites. The age of the meteorites has been accurately measured using $^{207}\mathrm{Pb}/^{206}\mathrm{Pb}$ ratios, to be 4.565 ± 0.005 Gyr. It follows that the Sun cannot have formed later than 4.59 Gyr ago, nor earlier than 4.55 Gyr ago (i.e., $4.565 + 3 \times 0.005 + 0.011$ Gyr, or $4.565 - 3 \times 0.005$ Gyr, at the 3-σ level). This total solar age estimate of, in effect, $t_\odot = 4.57 \pm 0.01$ Gyr is in agreement with the total solar (and solar system) age $\tau_{ss} = 4.53 \pm 0.03$ Gyr inferred previously by Guenther (1989) from a formation age of 4.53 ± 0.02 Gyr (Wasson 1985) for the meteorites and planets.

Our solar models were started relatively high on the pre-main-sequence Hayashi track, with central temperatures below 10^6 K; note that the ages $t_\odot$ of all our models are quoted relative to this pre-main-sequence starting point, which is within a few Myr of the solar formation age constrained by the meteoritic ages discussed above. A relatively high value of $t_\odot = 4.6$ Gyr was used for the reference standard solar model (cf. the observationally inferred value $t_\odot = 4.57 \pm 0.01$ Gyr from the previous paragraph). To get a reliable estimate of the sensitivity of the models to the solar age uncertainty, variant models were computed with ages differing by very large amounts, namely, $t_\odot = 4.5$ and 4.7 Gyr.

From our Hayashi track starting point, it takes only ~ 3 Myr for the luminosity on the pre-main-sequence to drop below 1 $L_\odot$ (i.e., below the present solar luminosity), but much longer, namely an additional 40 Myr, to reach the zero-age main sequence (ZAMS) — we have defined the ZAMS as the stage where the pre-main-sequence contraction terminates and the Sun begins to expand slowly, as nuclear burning in the core (rather than gravitational contraction) supplies essentially all of the solar luminosity. For the next ~ 50 Myr on the early main sequence, evolution is fairly fast, as $p +$ C reactions burn the initial carbon to nitrogen near the Sun's center, resulting in a short-lived convective core. Subsequently, the central carbon and nitrogen abundances approach their CN-cycle equilibrium values, the convective core disappears, and the Sun settles down to burn hydrogen mainly via the pp-chain reactions. Note that the pre-main-sequence timescale implies that the *total solar age* $t_\odot$ used in this paper can be converted into a *main sequence* solar lifetime by subtracting about 0.04 Gyr — this was also pointed out by Guenther (1989).

Helioseismology: We compared our solar models to profiles of the solar sound speed $c_\odot$, density $\rho_\odot$, and adiabatic index $(\Gamma_1)_\odot$ obtained from the helioseismic reference model of Basu et al. (2000)[6], which they

[6]From the denser-grid machine-readable form of their Table 2, at http://www.sns.ias.edu/~jnb/

obtained by inversion from the helioseismic frequency observations. In the inversion process, a standard solar model is required, but Basu et al. (2000) demonstrated that the resulting $c_\odot$ and $\rho_\odot$ profiles of the helioseismic reference model are relatively insensitive to uncertainties in the standard solar model used for this purpose (except for uncertainties in $R_\odot$, as discussed in § 3.1). They estimated a net uncertainty of few parts in 10^4 for the sound speed $c_\odot$ and adiabatic index $(\Gamma_1)_\odot$, and a few parts in 10^3 for the density $\rho_\odot$. However, in the Sun's core ($r \lesssim 0.1\ R_\odot$), systematic uncertainties in the helioseismic sound profile are increased by a factor of ~ 5; this was demonstrated by Bahcall et al. (2001), who compared helioseismic inversions of different helioseismic data sets. We used their comparison to estimate the r-dependence of the systematic error in $c_\odot$ in the core and in the convective envelope (namely, a fractional systematic error decreasing linearly from 0.0013 at $r = 0.05\ R_\odot$ to 0.0003 at $r = 0.2\ R_\odot$, constant from there to $r = 0.72; R_\odot$, then increasing linearly to 0.00052 at $r = 0.94; R_\odot$). For $c_\odot$, this systematic error can be significantly larger than the statistical errors quoted in the Table 2 of Basu et al. (2000), and we combined the two in quadrature to get the fractional error (σ_c/c) for the purpose of calculating weighted rms differences — the rms fractional difference in c is given by $\left(\left\{\sum[(\Delta c/c)/(\sigma_c/c)]^2\right\} / \left\{\sum[1/(\sigma_c/c)]^2\right\}\right)^{1/2}$. For $(\Gamma_1)_\odot$ and $\rho_\odot$, the systematic errors are comparable to or smaller than the statistical ones, and the statistical errors sufficed for calculating weighted rms differences.

3. Results and Discussion

3.1. Sound Speed and Density Profiles

We present in Figures 1 through 7 profiles of the adiabatic sound speed differences $\delta c/c \equiv (c_\odot - c_{model})/c_\odot$; profiles of the density differences $\delta\rho/\rho \equiv (\rho_\odot - \rho_{model})/\rho_\odot$ are available online[7]. For our equation of state comparison, we also considered the equivalent fractional difference in the adiabatic index Γ_1. Note that we use "δ" to denote differences between the helioseismic profile and one of our models, and "Δ" to denote differences between two of our models with different input parameters — the "δ" values are the profiles plotted in our figures, while the "Δ" values refer to the difference between one plotted curve and another.

The theoretical sound speeds c_{model} and densities ρ_{model} are from our computed reference standard solar model and from our variant standard solar models. Our reference standard solar model used current input parameters, as discussed in § 2; our variant standard solar models comprised standard solar models with one or more input parameters varied within the permitted range. We present all our sound speed and density profiles in terms of differences relative to the observed helioseismic reference profiles of Basu et al. (2000). This choice of presentation not only allows one to see the effects of the uncertainties in the input parameters, but also shows which choice of input parameters agrees best with the helioseismic observations. Our "OPALeos-lowT" model (discussed in more detail below) is the one most nearly comparable to the "STD" model of Basu et al. (2000), and yields similar $\delta c/c$ and $\delta\Gamma_1/\Gamma_1$ curves, as may be seem by comparing their Figures 2 and 3 to our Figure 1. Their models fit the solar sound speed profile somewhat better than our models do, but not significantly so, considering the size of the effects (discussed in detail further below) that result from reasonable variations in the input parameters of the solar model. We made no attempt to compare our solar models in the region outside $r = 0.943\ R_\odot$, the last point on the helioseismic profiles of Basu et al. (2000) — the reason that this *is* their outermost point is that significant systematic uncertainties

[7] http://www.krl.caltech.edu/~aib/papdat.html

arise in inversions near the solar surface (see, e.g., Di Mauro et al. 2002). However, we *have* compared the OPAL and MHD equation of state in this region, as have some other investigators (see, e.g., Guzik & Swenson 1997; Richard et al. 1998; Basu et al. 1999; Gong et al. 2001a; Di Mauro et al. 2002); this is discussed in detail further below.

Rotation effects: The prominent peak in $\delta c/c$ at $r \sim 0.7\ R_\odot$ visible in Figure 1a is due to the neglect of rotation-induced mixing just below the base of the solar convective envelope, as has been shown by a number of investigators who have included parameterized rotational mixing (see, e.g., Richard et al. 1996; Brun, Turck-Chièze, & Zahn 1999; Basu et al. 2000; Bahcall et al. 2001; Turck-Chièze et al. 2001b). There are significant uncertainties in the physical processes that lead to rotation-induced mixing. However, all of these investigators agree that rotational mixing is capable of smoothing out the peak at $r \sim 0.7\ R_\odot$, and that this has a relatively small effect on the sound speed elsewhere in the Sun (a fractional change of less than 0.001). For example, Bahcall et al. (2001) found that including "maximal" rotational mixing spread out this peak over the region $0.3\ R_\odot \lesssim r \lesssim 0.7\ R_\odot$, eliminating the prominent peak but worsening the agreement with the helioseismological sound speed profile by about 0.001 in much of the solar interior ($0.3\ R_\odot \lesssim r \lesssim 0.6\ R_\odot$). The "minimal" mixing model of Richard et al. (1996) yielded much the same result, as did similar models of other authors (Gabriel 1997; Brun et al. 1999; Turck-Chièze et al. 2001b). As far as the sound speed and density profiles in the core and the convective envelope are concerned, rotational mixing below the base of the convective envelope should have no significantly effect, as shown by the above authors.

Since the prominent peak at $r \sim 0.7\ R_\odot$ results from the neglect of rotational mixing, we did not require agreement in this region between profiles from our theoretical models and profiles inferred from the helioseismic observations. Nor did we require agreement in the inner core region, since the present helioseismic observations still result in large uncertainties in the inferred profiles there; for example, as shown by Bahcall et al. (2001), the use of a different helioseismic dataset could remove the the sharp upturn in $\delta c/c$ for $r \lesssim 0.1\ R_\odot$ in Figure 1a (and even convert it into a downward trend). On the other hand, we aimed for agreement in the regions $0.1\ R_\odot \lesssim r \lesssim 0.6\ R_\odot$ and $0.72\ R_\odot \lesssim r \lesssim 0.94\ R_\odot$, where disagreements are due to imperfections in the input physics or uncertainties in the observed solar parameters. This is demonstrated by our variant models, and by the variant models of other investigators (see, e.g., Morel et al. 1997; Guzik & Swenson 1997; Richard et al. 1998; Basu et al. 2000; Gong et al. 2001a; Neuforge-Verheecke et al. 2001a,b).

Convergence accuracy effects: The accuracy with which the model is converged to the solar radius, luminosity, and Z/X values can affect the sound speed profiles. The extent to which this occurs depends on the accuracy of the convergence, and on the sensitivity of the profiles to variations in $R_\odot$, $L_\odot$, and Z/X (these are discussed in detail below). Our convergence accuracy resulted in effects no larger than a few parts in 10^5 on the sound speed in the solar interior ($r \lesssim 0.6\ R_\odot$). In the convective envelope, where the sound speed is quite sensitive to $R_\odot$, the effect was typically less than a part in 10^4, but could be as high as a few parts in 10^4 for the few models with the worst convergence in $R_\odot$.

Note that the sound speed profile in most of the solar convective envelope ($0.72\ R_\odot \lesssim r \lesssim 0.94\ R_\odot$) is sensitive mainly to the equation of state and to the solar radius, with other uncertainties having only a minor effect there, as can be seen by considering this subregion in Figures 1 through 7.

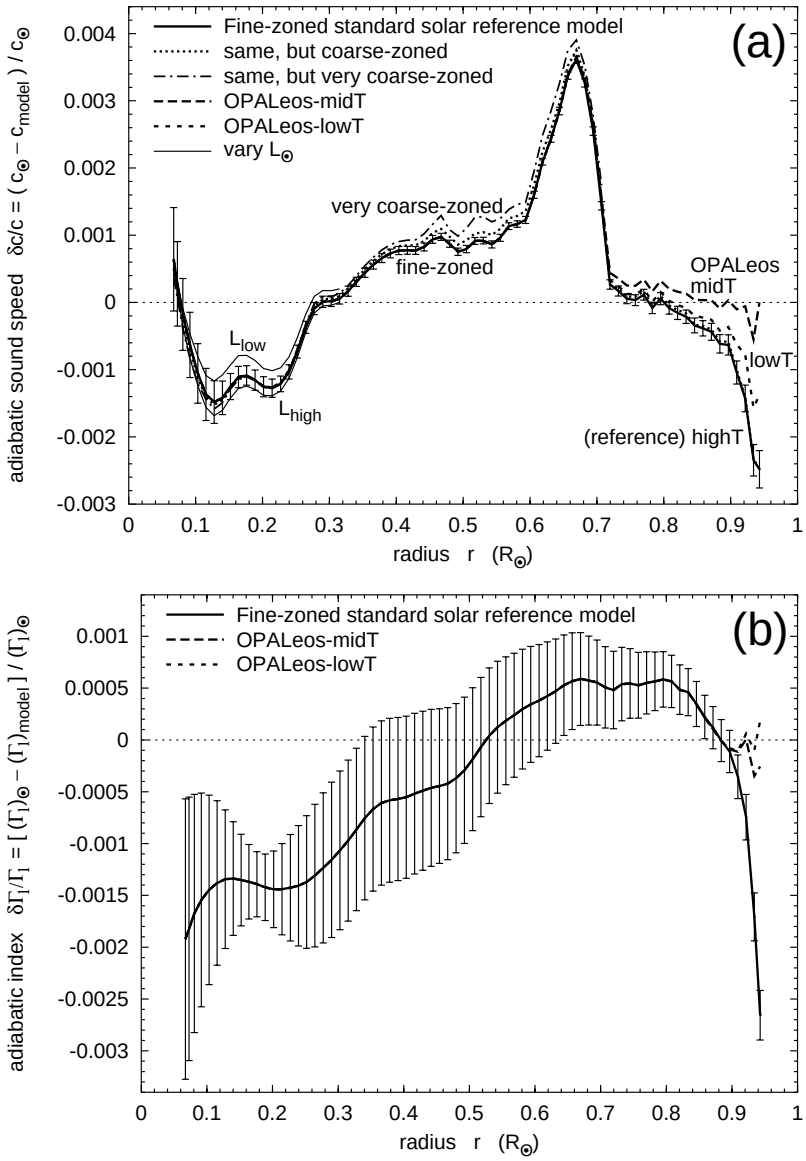

Fig. 1.— Changing the zoning, the outer-envelope equation of state, or the solar luminosity: the effects on (a) the adiabatic sound speed c, and (b) the adiabatic index Γ_1. The reference standard solar model (*thick solid line*: errorbars give *statistical error only*, for the inferred helioseismic profile) switches from the OPAL to the MHD equation of state for $\log \rho \lesssim -2$ (i.e., $r \gtrsim 0.94\ R_\odot$ or $\log T \lesssim 5.5$). The "OPALeos-midT" (*short-dashed line*) and "OPALeos-lowT" (*dashed line*) models have the equation-of-state switchover at $\log T \approx 4.0$ and $\log T \approx 3.75$, respectively. The *thin solid lines* show the effects of using the maximum ("L_{high}") and minimum ("L_{low}") values of $L_\odot$; for clarity, these are shown only for the region $r < 0.3\ R_\odot$ where there is a visible effect.

Zoning effects: We investigated the effects of using two different zonings. Our coarse-zoned models had about 2000 spatial zones in the model, and about 200 time steps in the evolution from the zero-age main sequence to the present solar age (plus about 800 time steps on the pre-main-sequence). These values are comparable to those used by most authors for solar models, although many authors use more complex algorithms than we did to compute changes between one timestep and the next (allowing the use of fewer main-sequence timesteps at the cost of more CPU-time per timestep), and some authors ignore the pre-main-sequence evolution entirely (or use less stringent accuracy conditions there). Typically, we ran solar evolutionary sequences (iteratively improving the input parameters Z_0, Y_0, and α) until our coarse-zoned models were converged to match the solar luminosity and radius to about a part in 10^5, and the solar surface Z/X to a part in 10^4; a few cases where convergence was slow were nearly 10 times worse. Our fine-zoned models had 10 000 spatial zones and took 1500 main-sequence time steps (plus 6000 pre-main-sequence time steps) — a factor of 5 increase in both spatial and temporal precision — and were typically converged to better than a part in 10^5 for $R_\odot$ and $L_\odot$, and a few parts in 10^5 for Z/X. We also tested some *very* coarse-zoned models, with 1000 spatial zones, 100 main-sequence time steps (plus 600 pre-main-sequence time steps), and convergence to the solar parameters of a few parts in 10^4. (A coarse-zoned converged solar model took a few hours of CPU-time on a fairly high-performance ES40 computer, as compared to a few days of CPU-time for a fine-zoned converged model; these times were roughly tripled on a 450 Mhz Pentium III PC.)

Figure 1a shows that the fine zoning made only a very modest improvement relative to the coarse-zoned case, less even than the statistical errors in the sound speed and density profiles obtained from helioseismic inversions. Even the *very* coarse-zoned test case did not do too badly: in the solar interior, it differs from the fine-zoned case by no more than 0.0004 in the sound speed profile and 0.003 in the density profile (amounts comparable to the systematic uncertainties in the helioseismic inversion) — the rms differences (over the entire Sun) are even smaller, namely $\mathrm{rms}\{\Delta c/c\} \approx 0.0003$ and $\mathrm{rms}\{\Delta\rho/\rho\} \approx 0.002$. The coarse-zoned model did about 3 times better still, with rms differences relative to the fine-zoned case of $\mathrm{rms}\{\Delta c/c\} \approx 0.0001$ and $\mathrm{rms}\{\Delta\rho/\rho\} \approx 0.0008$. Zoning changes had *no* effect on the adiabatic index Γ_1 (the coarse-zoned Γ_1 curves were not plotted in Fig. 1b, since they would be precisely superimposed on the fine-zoned curves). Additional tests demonstrated that changes in the coarseness of zoning always led to the *same* negligibly small systematic shift in solar interior sound speed and density values (although inaccuracies in matching the observed solar surface parameters could lead to slightly larger random variations in the convective envelope region $r \gtrsim 0.7\ R_\odot$). We therefore felt justified in running most of the models with our coarse zoning. Note that Morel et al. (1997), with about 1000 spatial zones, 60 main-sequence time steps, and convergence to present solar surface parameters of a part in 10^4 (similar to our very-coarse-zoned case), claimed a numerical internal accuracy of 0.0005 in the sound speed, similar to what we found for our very-coarse-zoned case.

Equation-of-state effects: Gong et al. (2001a) compared four current equations of state: their own MHD equation of state (Däppen et al. 1988), the OPAL equation of state (Rogers et al. 1996), the CEFF equation of state (Christensen-Dalsgaard & Däppen 1992), and the SIREFF equation of state Guzik & Swenson (1997). In each case, they used the approximation of a 6-element composition mixture (H, He, C, N, O, Ne) with the same composition as in the OPAL equation of state of Rogers et al. (1996). For $3.7 \lesssim \log T \lesssim 6$, at corresponding solar densities but *without* the usual "τ-correction" that eliminates the short-range divergence in the Debye-Hückel potential, Gong et al. (2001a) find OPAL – MHD differences in the equation of state of $\Delta P/P \leq 0.0005$, $\Delta\chi_\rho \leq 0.005$, $\Delta\chi_T \leq 0.007$, and $\Delta\Gamma_1 \leq 0.004$, with differences several times smaller at $6 \lesssim \log T \lesssim 7$, and comparable differences between other pairs of equations of state — recall that $\chi_\rho \equiv (\partial \ln P/\partial \ln \rho)_T$, $\chi_T \equiv (\partial \ln P/\partial \ln T)_\rho$, and the adiabatic index is $\Gamma_1 \equiv (\partial \ln P/\partial \ln \rho)_s$.

With the usual "τ-correction," but for a pure hydrogen-helium mixture ($Z = 0$), they find much larger differences: $\Delta P/P \lesssim 0.002$, $\Delta\chi_\rho \lesssim 0.02$, $\Delta\chi_T \lesssim 0.03$, and $\Delta\Gamma_1 \lesssim 0.008$.

Guzik & Swenson (1997) compared the effect in different solar *models*, finding roughly the same OPAL – MHD difference as the last of the above comparisons (namely, the case with the "τ-correction"), except that they find a much larger difference in the pressure; in the region $r \gtrsim 0.95\ R_\odot$ (i.e., $\log T \lesssim 5.5$), they find $\Delta P/P \leq 0.014$, $\Delta C_p/C_p \leq 0.036$, and $\Delta\Gamma_1 \lesssim 0.006$. Note that these differences include the effects of slightly different temperature, density, and composition profiles in the different solar models (which may either increase or decrease the differences in the thermodynamic quantities, since the solar models are re-adjusted to reproduce the present solar luminosity, radius, and surface composition).

We performed our own OPAL – MHD comparison, at *fixed* temperature, density, and composition grid-points in the equation of state tables — the same comparison as that performed by Gong et al. (2001a). Our results are consistent with those of Guzik & Swenson (1997); for a typical solar $\{T, \rho\}$ profile in the outer envelope region, we found $\Delta P/P \leq 0.017$, $\Delta C_v/C_v \leq 0.03$, $\Delta\chi_\rho \leq 0.015$, $\Delta\chi_T \leq 0.032$, and $\Delta\Gamma_1/\Gamma_1 \leq 0.006$.

The MHD equation of state is obtained in a fully self-consistent manner from the free energy; inaccuracies can arise only from deficiencies in the formulas used to obtain the free energy (Däppen et al. 1988; Gong, Däppen, & Zedja 2001b). However, for the OPAL equation of state (Rogers et al. 1996), we found that there were significant inconsistencies when we compared their tabulated values of Γ_1, $\Gamma_2/(\Gamma_2 - 1)$, and $(\Gamma_3 - 1)$ to values calculated from their tabulated values of P, C_v, χ_ρ, and χ_T. In the solar core, these inconsistencies are very small (a few parts in 10^4), but in the outer envelope ($r \gtrsim 0.94\ R_\odot$, or $\log T \lesssim 5.5$) we found inconsistencies as large as 3% at grid-points that would be used in the OPAL interpolation formulae when computing thermodynamic quantities (although the grid-points *nearest* to the solar $\{T, \rho\}$ locus have inconsistencies of less than 1%). Generally, the size of these inconsistencies varied smoothly in the OPAL grid, but in at least a few positions a few grid spacings away from the solar $\{T, \rho\}$ locus, there were sharp "spikes" where one of the thermodynamic quantities had a "glitch" (an error of several percent) at a just a couple of adjacent density and/or temperature points. In addition, for 4 of the 8 lowest OPAL T-grid points (at $3.71 \lesssim \log T \lesssim 3.77$), there is a "sawtooth" error: at every second density value, the tabulated quantities are shifted systematically relative to the values at neighboring densities and temperatures. These shifts can be as large as 1% at low densities for C_v and χ_T, and are always of order 0.1% for P.

A new OPAL 2001 equation of state has recently become available[8] (see also Rogers 2000, 2001), which includes relativistic electron effects and extends to both lower temperatures and higher densities then the original OPAL equation of state. Preliminary tests indicate that this OPAL 2001 equation of state has larger but smoother inconsistencies in its tabulated thermodynamic quantities, with few or no glitches, except in the extended high-density region (where there are some very large ones) and at the 2 lowest T-grid points ($\log T < 3.35$).

Gong et al. (2001a) found that the changing from a 6-element composition mixture to a 15-element mixture has an effect an order of magnitude smaller than the OPAL – MHD differences (we also performed such tests, and came to the same conclusion). They nonetheless recommended the use of at least a 10-element mixture for the best accuracy in an equation of state. They also noted a couple of minor deficiencies in the MHD equation of state that "moves it away from both helioseismically determined values and OPAL" (Gong et al. 2001a).

[8] ftp://www-phys.llnl.gov/pub/opal/eos2001/

Morel et al. (1997) compared solar *models* with the OPAL equation of state to ones with the CEFF equation of state, and found a small but non-negligible effect: sound speed differences $\Delta c/c$ of slightly over 0.001 and density differences $\Delta\rho/\rho$ up to 0.01. Note that they had set the value of Z_{eos} used in their equation of state to a fixed value of 0.019; however, since the equation of state is only weakly sensitive to Z, this should have only a minor effect on their models, and should not affect their comparison of the two equations of state. In general, the temperature, density, and composition profiles would *all* be slightly different between solar models with different equations of state, since the input parameters Z_0, Y_0, and α are adjusted individually for each solar model to obtain the best fit to the present solar luminosity, radius, and surface composition.

Guzik & Swenson (1997) presented more extensive solar model comparisons, comparing both their own SIREFF equation of state and the MHD equation of state to the OPAL equation of state (they too used a fixed Z_{eos}, of 0.02, but again this should not affect the comparison). They likewise found an effect $\Delta c/c \leq 0.001$ at $r \lesssim 0.95\ R_\odot$ (with differences up to 0.004 near the surface). They also presented differences between the values of the pressure P, specific heat at constant pressure C_p, internal energy U, and adiabatic index Γ_1. As mentioned above, near the solar surface ($r > 0.95\ R_\odot$) differences between models with different equations of state were relatively large, of order 1%. However, for $r \lesssim 0.9\ R_\odot$ Guzik & Swenson (1997) reported OPAL $-$ MHD differences between their solar models of $\Delta P/P \leq 0.0015$, $\Delta U/U \leq 0.002$, $\Delta\Gamma_1/\Gamma_1 \leq 0.0007$, and $\Delta C_p/C_p \leq 0.006$; the OPAL$-$SIREFF differences were slightly smaller for C_p, slightly larger for P and U, and much larger (a factor of ~ 3) for Γ_1. For $r \gtrsim 0.3\ R_\odot$, the SIREFF value of Γ_1 has several relatively large "wiggles" (fractional variations $\sim \pm 0.002$) relative to either OPAL or MHD. On the other hand, most of the difference in the core, and perhaps some difference in the average trend further out, may be due to the fact that SIREFF includes relativistic electron effects, while MHD and OPAL do not — although they *are* included in the *new* OPAL 2001 equation of state (Rogers 2000, 2001), and have recently been added to the MHD equation of state by Gong et al. (2001b).

Elliot & Kosovichev (1998) estimated that inclusion of relativistic effects would reduce the MHD or OPAL value of Γ_1 by a fraction 0.002 at $r \approx 0.1\ R_\odot$, this correction growing smaller with increasing r, to reach 0.001 at $r \approx 0.3\ R_\odot$ and zero near the solar surface. They pointed out that such a shift in Γ_1 for models using the OPAL or MHD equation of state would significantly improve the agreement in the solar interior with the inferred helioseismic Γ_1 profile. Certainly, if such a correction were applied to our Γ_1 curve in Figure 1b, the model profile would agree with the helioseismic profile within the statistical errors for all $r \lesssim 0.6\ R_\odot$ (recall that decreasing a model quantity shifts the curve upwards in the figures). Recently, Gong et al. (2001b) confirmed that adding relativistic electron effects to the MHD equation of state yields a change in Γ_1 very close to that estimated by Elliot & Kosovichev (1998).

The adiabatic sound speed is defined as $c = (\Gamma_1 P/\rho)^{1/2}$; changes in the solar ratio of P/ρ would result not only from changes in the equation of state but also from readjustments of the solar structure in response to these changes, so it is not obvious a priori what effect relativistic corrections would have on the sound speed. Consideration of the effect from Γ_1 alone suggest that relativistic corrections might reduce the slope at $r \lesssim 0.5\ R_\odot$ in the $\delta c/c$ curve of Figure 1a. The sound speed differences presented by Guzik & Swenson (1997) for their OPAL$-$SIREFF comparison suggest that this would in fact be the case, and that a fractional decrease of order 0.001 in the sound speed c_{model} near the Sun's center (i.e., an increase of 0.001 in $\delta c/c$ there) would result from relativistic corrections to the OPAL equation of state.

Richard et al. (1998) compared solar models with the OPAL and MHD equations of state, looking at the value of Γ_1 in the convective envelope ($0.72\ R_\odot \lesssim r \lesssim 0.98\ R_\odot$); they found that the OPAL equation of state appeared to perform slightly better there. This is not very surprising; what is perhaps more surprising is how well the MHD equation of state does in the solar interior, since it was only originally designed to be

accurate for $\rho \lesssim 10^{-2}$ g cm^{-3} (D. Mihalas 1999, private communication; see also Däppen et al. 1988; Gong et al. 2001a) — note that this ρ condition corresponds to $r \gtrsim 0.94\ R_\odot$ and $\log T \lesssim 5.5$ in the Sun. We investigated the effect of changing the equation of state only in this outer region where both are expected to be valid. Note that, while the OPAL *opacity* tables are unreliable for $\log T \lesssim 4$ due to their neglect of molecular opacities, the OPAL *equation of state* tables include molecular hydrogen effects, and should be reasonably accurate down to their lower tabulation limit of $\log T = 3.699$ (Rogers et al. 1996).

Basu et al. (1999) considered the outer part of the solar convective envelope ($0.8\ R_\odot \lesssim r \lesssim 0.99\ R_\odot$); they used a helioseismic inversion to study *intrinsic* Γ_1 differences relative to the solar values, where $(\delta\Gamma_1/\Gamma_1)_{int}$ is only that part of the difference that is ascribed to the equation of state in the inversion. They found that the OPAL Γ_1 value was preferable to the MHD value for $r \lesssim 0.97\ R_\odot$. Both equations of state did relatively well in the inner envelope, with $(\delta\Gamma_1/\Gamma_1)_{int} \lesssim 0.0005$; but near the solar surface both yielded a relatively large (negative) peak with $(\delta\Gamma_1/\Gamma_1)_{int} \sim 0.004$. This peak was deeper in for the MHD equation of state (at $r \sim 0.96\ R_\odot$, as compared to $r \sim 0.975\ R_\odot$ for OPAL), and also wider (reaching in to $r \sim 0.9\ R_\odot$, as opposed to $r \sim 0.95\ R_\odot$ for OPAL). Di Mauro et al. (2002) used recent observations of high-degree modes to perform a similar comparison, finding essentially the same result, though with a slightly higher peak difference $(\delta\Gamma_1/\Gamma_1)_{int} \sim 0.0055$ near the surface. Our Figure 1b plots the *total* Γ_1 differences rather than the intrinsic ones, but it is nonetheless likely that the sharp downturn in our MHD $\delta\Gamma_1/\Gamma_1$ profile (solid curve) at $0.9\ R_\odot \lesssim r \lesssim 0.94\ R_\odot$ corresponds to the inner edge of this "peak" in the MHD disagreement.

Our reference standard solar model used the OPAL equation of state in the interior regions, switching over to the MHD equation of state in the outer envelope; this switchover was performed gradually over the region $-1.5 > \log \rho > -2$ (corresponding to $0.89\ R_\odot < r < 0.94\ R_\odot$ and $5.8 > \log T > 5.5$ in the present Sun). We compared this reference standard model with two cases where the switchover occurred even further out in the envelope: a case "OPALeos-midT" where the switchover occurred for $4.0 > \log T > 3.9$, and a case "OPALeos-lowT" where the switchover occurred for $3.75 > \log T > 3.7$. In this latter "OPALeos-lowT" case, the MHD equation of state is used only outside the Sun's photosphere, and thus has negligible effect on the main sequence evolution. On the other hand, any artifacts induced by the switchover might be smaller in the former "OPALeos-midT" case, since differences between the two equations of state are significantly less near $\log T = 4$ than near $\log T = 3.7$ (although any such artifacts should be small in any case, comparable to effects of the inconsistencies in the OPAL equation of state, as discussed in § 2).

Figure 1 shows that, as one would expect, changing the equation of state in the outer envelope alone has no effect on the interior, and in fact there is only a minor effect in that part of the convective envelope where the equation of state remains unchanged. (This also demonstrates that any artifacts from the equation of state switchover do not affect the solar interior, and also have *at most* a minor effect on the convective envelope.) Since the effects were so small, we computed fine-zoned cases for this equation-of-state test; these are the ones presented in Fig. 1.

Note that Γ_1 is affected significantly *only* by variations in the equation of state.

Solar luminosity effects: Bahcall et al. (2001) tested the effect of 2-σ changes in the value of $L_\odot$ (namely, $\pm 0.8\%$) on their solar models, finding only a minor effect on neutrino fluxes and negligible effects on the other quantities they considered. For completeness, we made the same test with our own models, confirming their results. Figure 1a shows the effects on the sound speed of a solar luminosity 0.8% lower ("L_{low}") and 0.8% higher ("L_{high}") than the most recent value of 3.842×10^{33} erg s^{-1} (Bahcall et al. 2001; Fröhlich &

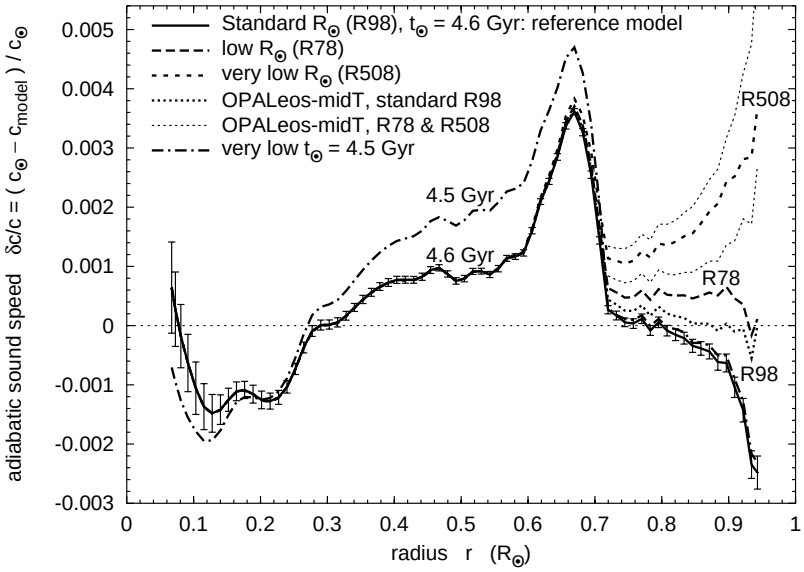

Fig. 2.— Effect on the sound speed of changing the solar radius or the solar age. The reference standard solar model (*thick solid line*) has the standard solar radius ($R_\odot = 695.98$ Mm: "R98") and a (high) solar age ($t_\odot = 4.6$ Gyr). The *dot-dashed line* shows the effect of using a *very* low solar age $t_\odot = 4.5$ Gyr (the observational value of $t_\odot = 4.57 \pm 0.01$ Gyr implies a total $3-\sigma$ age range only half as large as the difference between these cases). The *thick long-dashed line* shows the effect of using the low value of $R_\odot = 695.78$ Mm ("R78"), while the *thick short-dashed line* shows the effect of using the very low value of $R_\odot = 695.508$ Mm ("R508"). The *dotted lines* show the same radius comparisons for the "OPALeos-midT" case (in which the MHD equation of state is used only for $\log T \lesssim 4.0$, rather than $\log T \lesssim 5.5$). Note that variations in the solar radius would also affect the *inferred helioseismic sound speed profile*; this is discussed in the text, but the effects are *not* included in this figure.

Lean 1998; Crommelynck et al. 1996) — note that our reference standard solar model lies closer to L_{high} than to L_{low}, as it uses a slightly higher $L_\odot$ value than the most recent estimate (see § 2). To avoid confusion with other curves, the "L_{high}" and "L_{low}" curves are shown only in the region where they differ the most, namely, $r \lesssim 0.3\ R_\odot$; even in this region, a shift of 0.8% in $L_\odot$ produces a fractional change in the sound speed of less than 3 parts in 10^4, dropping to 1 part in 10^4 for $r > 0.3\ R_\odot$.

Solar radius effects: Basu et al. (2000) demonstrated that using a solar radius different from the standard value of $R_\odot = 695.98$ Mm could have a small but not completely insignificant effect on *both* the sound speed profile inferred from helioseismic inversions and that computed in solar models. They found that using the 0.03% smaller solar radius value $R_\odot = 695.78$ Mm (case "R78") suggested by the f-mode study of Antia (1998) would reduce the inferred helioseismic sound speed profile throughout the Sun by about the same small fraction, namely 0.0003 (nearly independent of position in the Sun); similarly, using the 0.07% smaller value $R_\odot = 695.508$ Mm (case "R508") suggested by the solar-meridian transit study of Brown & Christensen-Dalsgaard (1998) would reduce the inferred helioseismic sound speed profile by 0.0007. On plots such as ours of fractional differences $\delta c/c \equiv (c_\odot - c_{model})/c_\odot$, such a reduction in "$c_\odot$" would shift all the curves downwards by the given amounts. This shift has *not* been performed in Figure 2 — we only display

our c_{model} values relative to the $c_\odot$ values of Basu et al. (2000), so as to allow comparisons between different solar models — but this effect *has* been included in our quoted rms values relative to the Sun "rms$\{\delta c/c\}$" (see next paragraph, and Table 1). Basu et al. (2000) also calculated that a change in the solar radius would result in a non-uniform shift in the inferred helioseismic $\rho_\odot$ and $(\Gamma_1)_\odot$ profiles, by amounts comparable to the statistical errors in these quantities; although these shifts are barely significant statistically, in contrast to the shift in $c_\odot$, for completeness their effects have been applied to our rms values calculated relative to the helioseismic profiles for the "R78" and "R508" cases.

Figure 2 illustrates the effect on the sound speed of changing the value of $R_\odot$ from the standard "R98" case to the smaller "R78" and "R508" cases. Only in the convective envelope is the sound speed significantly affected, with the largest effect being near the solar surface. In the "peak" region just below the convective envelope, these "R78" and "R508" curves differ from the reference standard solar model by no more than a few parts in 10^4, and this difference drops to about a part in 10^5 for $r < 0.6\ R_\odot$. In the convective envelope ($r \gtrsim 0.72\ R_\odot$), the "R78" case is an improvement on the reference model (reducing envelope-only rms$_{env}\{\delta c/c\}$ from 0.0007 to 0.0004 when one includes the effect of the shift in the inferred helioseismic profiles), but the "R508" case is worse (rms$_{env}\{\delta c/c\} = 0.0011$). For the "OPALeos-midT" case, reducing the solar radius *always* worsens agreement in the convective envelope (rms$_{env}\{\delta c/c\}$ of 0.0003 is increased to 0.0009 or 0.0018 for "R78" or "R508," respectively). Figure 2 also shows that the effect on the sound speed profile of changes in the solar radius adds linearly to effects from changes in the envelope equation of state.

The overall rms and the rms in the interior are not much affected by variations in the solar radius, as may be seen from Table 1. However, if relativistic corrections had been included in the equation of state, the $\delta c/c$ profile in Figure 2 would probably have been less negative at $r \lesssim 0.3\ R_\odot$; an overall downward shift in the whole profile (such as results from the overall shift in the inferred helioseismic sound speed profile for smaller $R_\odot$ values) would then probably lead to some improvement in rms$\{\delta c/c\}$. However, the effect would still be much smaller than some of the other effects discussed below.

Solar age effects: Figure 2 demonstrates that the uncertainty in the solar age $t_\odot$ has only a very minor effect on the solar sound speed profile — note that the shift illustrated here, from $t_\odot = 4.6$ Gyr to 4.5 Gyr, is much larger than the observationally allowed range of solar ages, i.e., 4.55 Gyr $\lesssim t_\odot \lesssim$ 4.59 Gyr, as discussed in § 2. (These ages are defined to include the pre-main-sequence; main sequence ages can be obtained by subtracting 0.04 Gyr). The maximum allowed shift of 0.02 Gyr relative to the "best" solar age of 4.57 Gyr would yield negligibly small effects, namely, rms$\{\Delta c/c\} \approx 0.0001$ and rms$\{\Delta\rho/\rho\} \approx 0.001$, with maximum changes less than twice these values. Our results agree both qualitatively and quantitatively with the age sensitivity found in the recent work of Morel et al. (1997).

Low-temperature opacity effects: Uncertainties in the low-temperature molecular opacities would not be expected to have much effect — in a convective region, such as the solar convective envelope, the structure is almost independent of the local opacity. As expected, using the Sharp (1992) molecular opacities ("$\kappa_{\rm Sharp}$") below 10^4 K rather than the Alexander & Ferguson (1994) molecular opacities ("$\kappa_{\rm Alexander}$") led to essentially identical sound speed and density profiles — the "$\kappa_{\rm Sharp}$" case is thus not plotted in Figure 3. The rms differences are negligible, less than a part in 10^4 for the sound speed and less than a part in 10^3 for the density. Only pre-main-sequence lithium depletion was significantly affected (see § 3.4).

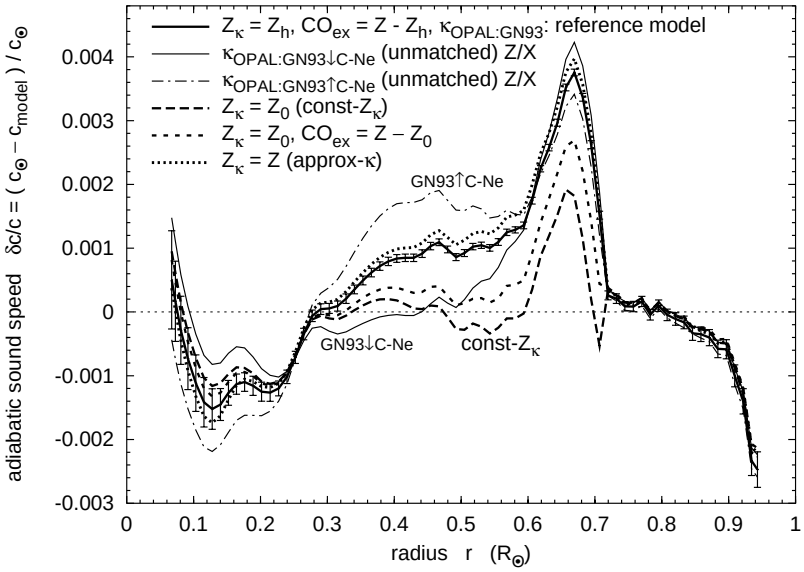

Fig. 3.— Effect on the sound speed of opacity interpolation choices. The *thin solid* and *dot-dashed lines* show the effects of opacities where the C, N, O, and Ne abundances were respectively decreased ("$\kappa_{\rm OPAL:GN93\downarrow C-Ne}$") or increased ("$\kappa_{\rm OPAL:GN93\uparrow C-Ne}$") by their quoted errors of 15%, but the value of Z/X was not re-adjusted to reflect these changes, so these cases are not self-consistent (compare to the self-consistent cases in Fig. 5 below). Using opacity tables at a single constant metallicity ("const-Z_κ:" *long-dashed line*) leads to large opacity errors and thus large sound speed errors, which cannot be fixed by interpreting the metallicity error as "excess-CO" (*short-dashed line*). However, ignoring the effect on the opacity of *relative* differences in the abundance profiles of the individual metals results in only minor errors ("approx-κ:" *dotted line*).

Interior opacity effects: Recently, Neuforge-Verheecke et al. (2001b) compared models using the 1995 OPAL opacities (Iglesias & Rogers 1996; Rogers et al. 1996) with models using an updated version of the LEDCOP opacities from Los Alamos (Magee et al. 1995); under solar conditions, these two sets of opacities differ by up to 6% (just below the base of the convective envelope), although the authors indicate that about half of this difference is due to interpolation errors (from different temperature grids on which the opacities are tabulated). They find fractional sound speed differences up to $\Delta c/c \sim 0.003$ between solar models using these different opacity tables. Morel et al. (1997) have also demonstrated the serious impact of opacity changes on the sound speed and density profiles of solar models; they compared the 1995 OPAL opacities with the less-precise 1992 OPAL opacities (Rogers & Iglesias 1992) (albeit with models that neglected diffusion), finding that the improved opacities made an improvement of up to 0.005 in the sound speed and up to 0.03 in the density (see their models S1 and S2). Basu et al. (2000) compared a model with the 1995 OPAL opacities and the OPAL equation of state (Rogers et al. 1996) to a model with the 1992 OPAL opacities and the cruder Yale equation of state (Guenther et al. 1992) with the Debye-Hückel correction (Bahcall, Bahcall, & Shaviv 1968) (their models did include diffusion); they likewise found an effect of up to 0.005 in the sound speed and up to 0.03 in the density, from the combination of these two changes in the input. We found that an even larger improvement of up to 0.007 in the sound speed resulted from changing from the even older Los Alamos (LAOL) opacities (Keady 1985, private communication) to the 1995 OPAL opacities, with an rms improvement of 0.004 as shown in Table 1 (there is also an improvement of up to 0.04 in the

density, with an rms improvement of 0.02) — however, such a large opacity change as this overestimates the uncertainty in the 1995 OPAL opacities (Rogers & Iglesias 1998).

As pointed out by Morel et al. (1997), neglecting the opacity changes that result from metallicity variations in the Sun would lead to significant errors — e.g., errors of up to 0.0015 in the sound speed. In our reference standard solar model, we did our best to account for these temporal and spatial variations in the opacity due to these composition changes from diffusion and nuclear burning. As discussed in § 2, the metallicity value Z_κ that we used for metallicity interpolation in the OPAL opacity tables was scaled according to the changes in the elements heavier than oxygen ("$Z_\kappa = Z_h$," where Z_h is proportional to the heavy element abundance). Several different methods were tested to account for the fact that changes in the CNO-element abundances (particularly in the solar core) are far from being proportional to changes in the heavy elements. As discussed in § 2, all such methods that we tested gave essentially identical results — even omitting the CNO-correction entirely had almost no effect, and only a negligible improvement resulted from a full "CNO-interpolation" case that included the full opacity effects of CNO abundance variations quite accurately (by interpolating among several separately-computed OPAL opacity tables with different CNO abundances). For our reference standard solar model, we simply assigned the sum of the non-proportional changes in the CNO abundances (namely, $Z - Z_h$) to the "excess carbon and oxygen" interpolation variable of the OPAL opacity tables (i.e., $\mathrm{CO}_{ex} = Z - Z_h = Z - Z_\kappa$).

An alternative approximation ("approx-κ") is to set $Z_\kappa = Z$ (i.e., to interpolate the OPAL opacity tables in the local metallicity Z, but ignore effects of variations in the makeup of Z). As shown in Figure 3, this approximation yields results almost identical to those of our reference standard solar model; rms differences are $\mathrm{rms}\{\Delta c/c\} \approx 0.0002$ and $\mathrm{rms}\{\Delta\rho/\rho\} \approx 0.001$, with maximum differences not very much larger. Morel et al. (1997) compared two different ways of estimating the value of Z_κ (both being similar but not identical to our "approx-κ" case); they likewise found only very minor differences in the sound speed between their two methods, but much larger effects on the density (see their models D3 and D12).

We also tested cases where OPAL opacities had been calculated for mixes in which the abundances of C, N, O, and Ne were either all increased by their quoted errors of 15% ("$\kappa_{\mathrm{OPAL:GN93}\uparrow\mathrm{C-Ne}}$") or decreased by this amount ("$\kappa_{\mathrm{OPAL:GN93}\downarrow\mathrm{C-Ne}}$"), relative to their abundances quoted by Grevesse & Noels (1993). Figure 3 illustrates an effect of up to 0.001 in the sound speed from such a change. However, we used a value of $Z/X = 0.0245$ for all of the models in Figure 3, which is not strictly consistent with such large abundance changes: since C, N, O, and Ne comprise the major portion of Z, a 15% change in their abundances should correspond to a change of $\sim 12\%$ in Z/X as well. We discuss such a self-consistent opacity-plus-composition-plus-Z/X variations under Z/X effects below.

Even when using the most up-to-date OPAL opacities, one can still get significant errors if one neglects the effect on opacity of Z-changes (primarily due to diffusion). The simplest case is to set $Z_\kappa = Z_0$ ("const-Z_κ"), where Z_0 is the protosolar metallicity; in effect, such a case uses only the OPAL opacity tables relevant to the protosolar metallicity and ignores the effect on the opacity of any subsequent changes in the metallicity. Figure 3 demonstrates that this "const-Z_κ" case yields errors of up to $\Delta c/c \sim 0.0015$ relative to the more accurate opacity interpolation of the reference standard solar model, in agreement with the results of Morel et al. (1997) (compare their models D10 and D12); the rms errors were $\mathrm{rms}\{\Delta c/c\} \approx 0.0010$ and $\mathrm{rms}\{\Delta\rho/\rho\} \approx 0.007$. One might attempt to fix up this neglect of metallicity variation by interpolation using the mildly CO-enhanced OPAL opacity tables, i.e., retaining a constant $Z_\kappa = Z_0$ for opacity interpolation purposes but setting CO_{ex} to the difference between Z_κ and the true value of Z that results from diffusion and nuclear burning, i.e., $\mathrm{CO}_{ex} = Z - Z_\kappa = Z - Z_0$. Figure 3 illustrates that this approximation is a slight improvement over the "const-Z_κ" case but still not very satisfactory: it still has rms errors of

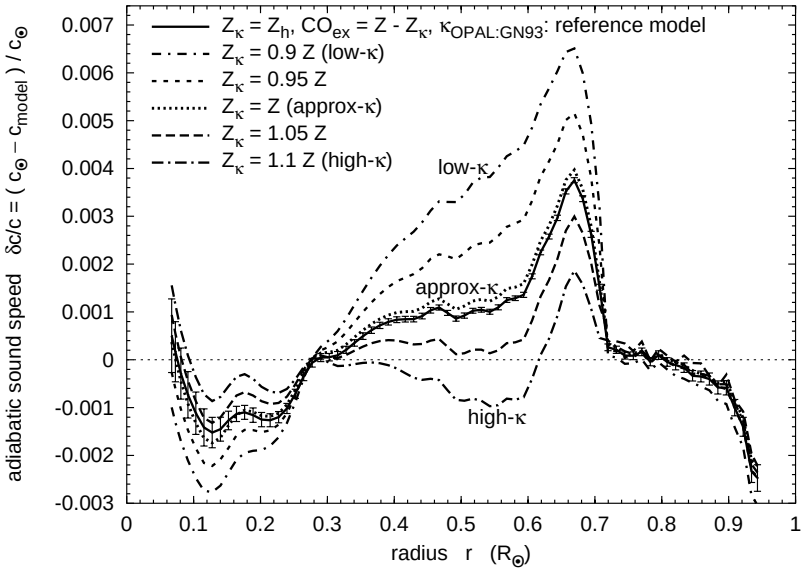

Fig. 4.— Effect on the sound speed of opacity uncertainties. The *dot-dashed lines* ("low-κ" and "high-κ") show the effect of a $\sim 10\%$ overall change in the opacities relative to the reference standard solar model (*thick solid line*), while the *dashed lines* show the effect of a $\sim 5\%$ overall change in the opacities.

rms$\{\Delta c/c\} \approx 0.0006$ and rms$\{\Delta\rho/\rho\} \approx 0.004$.

Interpolation errors can also arise from the finite grid spacing of the opacity tables in X, Z, T, and ρ. In creating the opacity interpolation routines, we tested the X- and Z-interpolation, finding that these should result in only minor errors (a fraction of a percent) in the opacity. The work of Neuforge-Verheecke et al. (2001b) suggests that T- and ρ-interpolation errors in the opacity can be larger, as much as a few percent.

In addition to errors introduced by methods of interpolating in opacity tables, one must consider the errors in the actual opacity values contained in the tables. Such opacity errors will in general be functions of temperature and density; also, different elements will have different errors. Rogers & Iglesias (1998) estimate that there is a 4% uncertainty in the 1995 OPAL opacities from effects neglected in their calculations — Neuforge-Verheecke et al. (2001b) point out that the $\sim$ 3% intrinsic differences between the OPAL and LEDCOP opacities are slightly less than this. Turcotte et al. (1998) showed that differences in the Rosseland mean opacities between 1992 and 1995 OPAL opacities do not exceed 7% over the run of temperature and density in the Sun's interior, and that these opacity differences yielded sound speed differences of up to 0.002 in their solar models. In addition, errors in the observed relative heavy element abundances in the solar envelope will translate into opacity errors, since different elements have somewhat different opacities. Rogers & Iglesias (1998) estimate that such abundance uncertainties correspond to opacity uncertainties of order 5% at temperatures where ionization effects of the relevant elements yield a large contribution to the opacity (e.g., near 2×10^6 K for oxygen or neon). Turcotte et al. (1998) found that taking into account the opacity effects due to changes in the relative abundances of all the individual elements in Z led to opacities that differed by up to 2% from the opacities tabulated for the standard scaled-solar metallicity, yielding sound speed differences of up to 0.001 and density differences up to 0.005 — these are several times larger than the effects discussed above that we found when testing effects of variations of C, N, and O relative to the heavier elements.

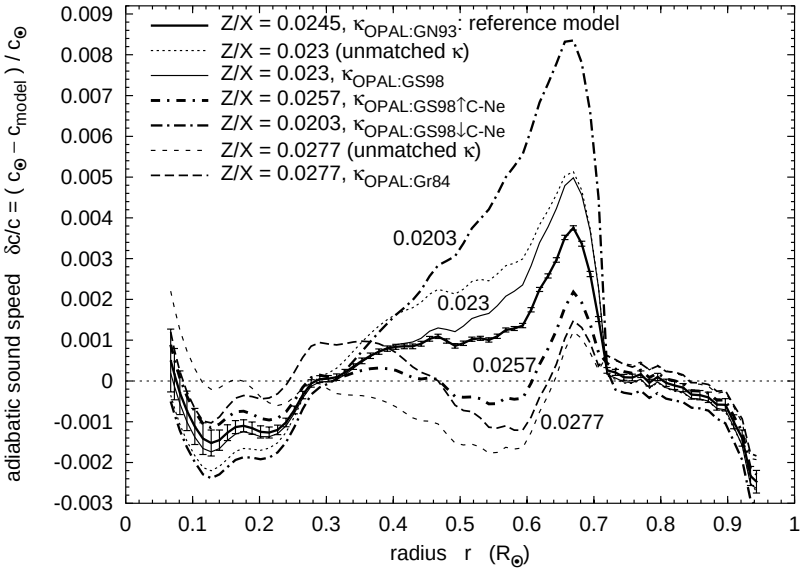

Fig. 5.— Effect on the sound speed of uncertainties in the observed solar surface composition. Relative to the reference standard solar model at $Z/X = 0.0245$ (*thick solid line*), switching to the more recent $Z/X = 0.023$ value of Grevesse & Sauval (1998) *without* including the corresponding changes in *relative* metal abundances (*thin dotted line*) has a larger effect than the full case with self-consistent abundances and opacities ("$\kappa_{\rm OPAL:GS98}$:" *thin solid line*); the same is true when considering the older $Z/X = 0.0277$ cases of Grevesse (1984) (*thin short-dashed line* vs. self-consistent "$\kappa_{\rm OPAL:Gr84}$" *thick long-dashed line*). Nonetheless, a self-consistent test of the uncertainties in the Grevesse & Sauval (1998) C, N, O, and Ne abundances (*thick dot-dashed lines*) shows a large effect (compare to the *thin solid line*).

We did not attempt detailed element-by-element variations of the OPAL opacities in our models; nor did we test the effect of opacity variations in limited density or temperature ranges. Instead, we obtained a rough estimate of the maximum possible effects of uncertainties in heavy-element opacities by making an overall shift in the metallicity value Z_κ used for interpolation in the OPAL opacity tables. Figure 4 illustrates the cases $Z_\kappa = 0.9\,Z$ ("low-κ"), $Z_\kappa = 0.95\,Z$, $Z_\kappa = Z$ ("approx-κ"), $Z_\kappa = 1.05\,Z$, and $Z_\kappa = 1.1\,Z$ ("high-κ"). The "low-κ" and "high-κ" cases correspond to an average shift in the opacities of order 10% over the solar interior relative to the "approx-κ" case ($2-5\%$ for $r \lesssim 0.4\ R_\odot$, $\sim 10\%$ for $0.4\ R_\odot < r < 0.7\ R_\odot$, $\sim 15\%$ for $0.7\ R_\odot < r < 0.92\ R_\odot$, and $\sim 5\%$ for $r > 0.92\ R_\odot$). As may be seen from Figure 4, such an opacity shift of order 10% yields sound speed changes of up to $\Delta c/c \sim 0.003$, with $\mathrm{rms}\{\Delta c/c\} \approx 0.0016$ and $\mathrm{rms}\{\Delta\rho/\rho\} \approx 0.014$. However, such a large opacity shift almost certainly overestimates the effects of opacity uncertainties. Rogers & Iglesias (1998) estimate that there is a 4% uncertainty in the 1995 OPAL opacities from effects neglected in their calculations, and it would be surprising if these yielded a uniform shift in the opacity throughout the Sun. Thus a better estimate of the effects of opacity uncertainties would be $\Delta c/c \sim 0.001$ and $\mathrm{rms}\{\Delta\rho/\rho\} \sim 0.005$.

Solar abundance (Z/X) effects: Our reference standard solar model used the observational value of $Z/X = 0.0245$ from Grevesse & Noels (1993), since their mixture was the one for which the standard OPAL opacity tables ("$\kappa_{\rm OPAL:GN93}$") were available. The short-dashed curve in Figure 5 demonstrates the effects of

using the Grevesse & Noels (1993) relative metal abundances with the corresponding "$\kappa_{\rm OPAL:GN93}$" OPAL opacities, but using a 13% higher value of $Z/X = 0.0277$, the older value that had been recommended by Grevesse (1984); the maximum sound speed difference relative to the reference standard solar model is $\Delta c/c \sim 0.0030$, with rms$\{\Delta c/c\} \approx 0.0018$ and rms$\{\Delta\rho/\rho\} \approx 0.017$. The dotted curve in Figure 5 illustrates a similar case with a 6% lower value of $Z/X = 0.023$, as recommended by the more recent work of Grevesse & Sauval (1998); it has maximum $\Delta c/c \sim 0.0016$, with rms$\{\Delta c/c\} \approx 0.0010$ and rms$\{\Delta\rho/\rho\} \approx 0.009$. (Note that most of the above effect comes from the different opacity that results from the changed solar Z value, as may be seen by comparing with the "high-κ" and "low-κ" curves in Fig. 3.) However, these comparisons are not strictly self-consistent, since it is the changes in the individual elemental abundances of the metals that add up to yield the changed Z/X ratio. Using the old abundance pattern of Grevesse (1984) and newly-computed OPAL opacities appropriate to it ("$\kappa_{\rm OPAL:Gr84}$") leads to the wide-dashed $Z/X = 0.0277$ curve in Figure 5, with a slightly smaller maximum sound speed difference (of 0.0025), and rms$\{\Delta c/c\} \approx 0.0014$ and rms$\{\Delta\rho/\rho\} \approx 0.011$. Similarly, using the Grevesse & Sauval (1998) abundance pattern and appropriate OPAL opacities ("$\kappa_{\rm OPAL:GS98}$") leads to the thin solid $Z/X = 0.023$ curve in Figure 5, reducing the maximum sound speed difference to 0.0012, with similarly reduced rms$\{\Delta c/c\} \approx 0.0006$ and rms$\{\Delta\rho/\rho\} \approx 0.004$.

Neuforge-Verheecke et al. (2001a) performed a comparison identical to this last case, finding essentially the same effect on the sound speed, both qualitatively and quantitatively (maximum effect ~ 0.0018). Morel et al. (1997) considered the effect of a 6% increase in Z/X, finding a maximum difference of 0.0007 in their sound speed and 0.003 in their density; this would imply a significantly lower sensitivity to Z/X than we found. This is probably due to the fact that the models in which they tested Z/X variations did not consider the effect on the opacities of the temporal and spatial variations in the heavy element abundances that arise from diffusion, but merely used opacities appropriate to a constant metallicity equal to the protosolar value ($Z_\kappa = Z_0$, as in our "const-Z_κ" case discussed above).

Strictly, the uncertainty resulting from observational solar abundance errors can be estimated by varying the solar abundance values of Grevesse & Sauval (1998) within their quoted uncertainties, obtaining OPAL opacities with these revised compositions, calculating the resulting Z/X values, and running solar models with these self-consistent sets of input values. We have done this for two cases. Rather than performing large numbers of random variations of the abundances, we tested a case which should give something close to the maximum effect. The elements C, N, O, and Ne not only comprise the major part of the metallicity but also have relatively large errors of $\sim 15\%$, and unlike other elements with large errors one cannot get a "better" value by using the meteoritic abundance instead. We therefore considered cases where C, N, O, and Ne were either all increased by 15% ($Z/X = 0.0257$, "$\kappa_{\rm OPAL:GS98\uparrow C-Ne}$") or all decreased by 15% ($Z/X = 0.0203$, "$\kappa_{\rm OPAL:GS98\downarrow C-Ne}$") — i.e., these self-consistent abundance variations correspond to 12% variations in Z/X. As illustrated in Figure 5, these cases lead to variations in the solar sound speed of up to 0.003 relative to the $Z/X = 0.023$ "$\kappa_{\rm OPAL:GS98}$" case, with rms$\{\Delta c/c\} \approx 0.0017$ and rms$\{\Delta\rho/\rho\} \approx 0.012$. Of all the "input" uncertainties that we considered, these uncertainties in the solar abundances have the largest impact.

Nuclear rate effects: Figure 6 demonstrates that the uncertainty in the ^{1}H$(p,\nu e^+)^2$H nuclear burning rate (the *pp* rate) has a significant impact on the solar sound speed. Our reference standard solar model used the recommended nuclear rates from the NACRE compilation (Angulo et al. 1999). These authors also supply "high" and "low" cases to indicate the allowed uncertainty range of each nuclear rate; in the case of the *pp* reaction, the high case is 8% above the recommended rate and the low case is 3% below it. We have tested the effects of nuclear rate uncertainties by computing variant standard solar models using high and low NACRE rate values. Figure 6 demonstrates that a high *pp* rate is preferable, if all

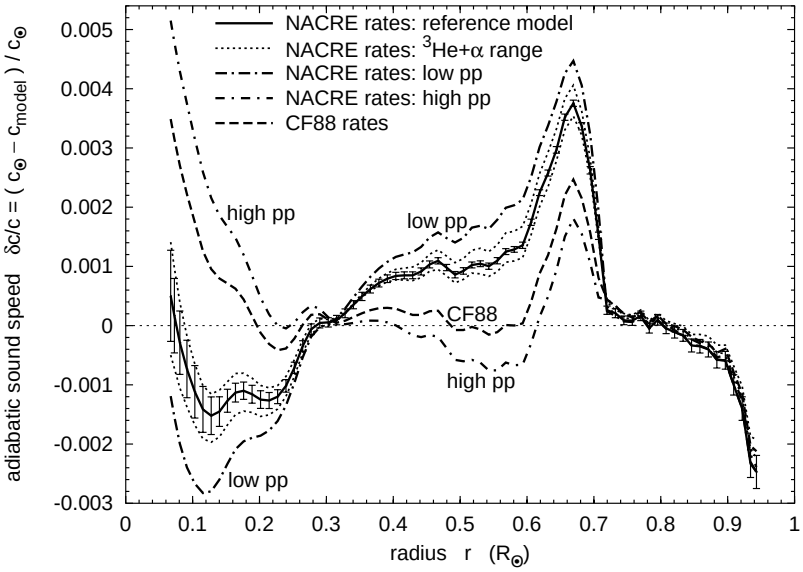

Fig. 6.— Effect on the sound speed of uncertainties in nuclear rates. The $\sim 5\%$ uncertainty in the basic *pp* rate (*dot-dashed lines*) has a much larger effect than the 20% uncertainty in the $^3\mathrm{He} + \alpha$ rate (*dotted lines*); other rate uncertainties have negligible effects, and are not plotted. The difference between the reference standard solar model using the NACRE rates (*solid line*) and the model using the Caughlan & Fowler (1988) rates ("CF88:" *dashed line*) is largely due to the higher *pp* rate adopted by the latter authors.

other parameters are kept constant: the high *pp* rate gives good agreement with the helioseismic reference profiles, except in the Sun's central regions where the helioseismic observations are the poorest. Our models indicate that a change of 5% in the *pp* rate yields changes of up to 0.003 in the sound speed, (0.0014 in the regions accurately probed by helioseismology, outside the core); the rms changes in such a case would be $\mathrm{rms}\{\Delta c/c\} \approx 0.0009$ and $\mathrm{rms}\{\Delta\rho/\rho\} \approx 0.018$. Antia & Chitre (1999) also tested the effects of changes in the *pp* rate on the helioseismic profiles, concluding that a relatively high *pp* rate is preferred, consistent with our results discussed above.

Figure 6 also demonstrates that the uncertainty of $\pm 20\%$ in the $^3\mathrm{He}(\alpha,\gamma)^7\mathrm{Be}$ reaction leads to only a minor effect: a maximum sound speed change of 0.001 (or 0.0003 outside the core), with $\mathrm{rms}\{\Delta c/c\} \approx 0.0002$ and $\mathrm{rms}\{\Delta\rho/\rho\} \approx 0.004$. Basu et al. (2000) considered the effect of setting the $^3\mathrm{He}(\alpha,\gamma)^7\mathrm{Be}$ rate to zero; they found large effects from such an unphysically extreme change. Setting the rate to zero is equivalent to a 100% change, 5 times as large as the 20% change that we considered; thus it is consistent that their published effect is about 5 times as large as ours.

We also tested the effects of the $\pm 6\%$ uncertainty in the $^3\mathrm{He}(^3\mathrm{He}, 2p)^4\mathrm{He}$ reaction and of the $\pm 30\%$ uncertainty in the $^{14}\mathrm{N}(p,\gamma)^{15}\mathrm{O}$ reaction (which determines the CNO-cycle rate). Such changes in these rates led to negligible effects on the sound speed and density profiles; we have not plotted these profiles in Figure 6, since they would be essentially superimposed on that of the reference standard solar model.

It is not surprising that the uncertainty in the *pp* rate has the largest effect on the sound speed and density profiles, since it is the basic rate that determines the overall p-p chain burning rate.

We also computed a model using the previous standard set of nuclear rates, namely, the Kellogg nuclear

rate compilation of Caughlan & Fowler (1988). The resulting sound speed and density profiles are shown in Figure 6. With us still in Kellogg, carrying out this work in an office directly below his long-time office, it is especially gratifying for us to see that Willy Fowler's last published *pp* rate yields such good agreement with the current helioseismic reference profiles (the largest differences being near the center, where the observations are least accurate).

Electron screening effects in nuclear rates: Gruzinov & Bahcall (1998) performed a careful quantum mechanical computation of the effects of electron screening on nuclear reactions in the Sun, and found that the Salpeter (1955) formula leads to only a very slight overestimate of the nuclear rates: 0.5% for the $p + p$ reaction, 1.7% for the $^3\mathrm{He} + {}^4\mathrm{He}$ reaction, 1.5% for the $p + {}^7\mathrm{Be}$ reaction, and 0.8% for the $p + {}^{14}\mathrm{N}$ reaction. Since these corrections are an order of magnitude smaller than the uncertainties given in the corresponding NACRE nuclear rates (Angulo et al. 1999), there was no point in considering separately the uncertainty in the screening corrections. Note that if one used the intermediate screening formulae (including the partial degeneracy correction) of Graboske et al. (1973), one would overestimate the nuclear reaction rates in the Sun by a further 1 to 3% relative to the weak screening formula — Gruzinov & Bahcall (1998) quoted a much larger effect in the opposite direction, but this was for a version of the Graboske et al. (1973) formulae that assumed completely degenerate electrons.

Shaviv & Shaviv (1996) suggested that electron cloud-cloud interactions would increase the electron screening factor in the exponent of nuclear rates by a factor of 2/3; this was based on a "fundamental misconception concerning the dynamics of the interaction" (Brüggen & Gough 1997). Carraro, Schäfer, & Koonin (1988) suggested that "dynamic screening" should reduce the Salpeter (1955) screening factor, since half of the screening effect comes from ions, which should not be able to adjust to the rapid motion of colliding/fusing nuclei. However, Gruzinov (1998) gave a general argument showing that in an equilibrium plasma there should be no such reduction, and Brown & Sawyer (1997) showed explicitly that such a modification of the Salpeter screening factor is exactly cancelled when one considers processes whereby Coulomb interactions with the colliding particles cause plasma excitations and de-excitations. Bahcall et al. (2002) point out that the more recent "dynamic screening" calculations of Shaviv & Shaviv (2000, 2001) seem likewise to be based on misconceptions.

Bahcall et al. (2002) showed several ways of deriving the fact that the Salpeter (1955) electron screening formula gives the correct leading term under weak screening conditions, and used the rigorous formulation of Brown & Sawyer (1997) to show that, in the Sun, corrections to this leading term are small (of order 1%). They also pointed out that Tsytovich's alternative "anti-screening" formula (Tsytovich 2000; Tsytovich & Bornatici 2000), which yields a reduction in nuclear rates rather than an increase, yields unphysical results in two different limits. Nonetheless, some authors (Fiorentini, Ricci, & Villante 2001; Weiss, Flaskamp, & Tsytovich 2001) have looked into the effects of using Tsytovich's alternative "anti-screening" formula, and have shown that it yields solar models that are not compatible with the helioseismic sound speed profile.

Non-Maxwellian ion velocity distributions: Coraddu et al. (1999) suggest that the high-energy tail of the Maxwellian ion velocity distribution may be slightly depleted in the Sun; to first order, they express this modified distribution by $f(E) \sim (kT)^{-3/2} e^{-E/kT - \delta(E/kT)^2}$, where they estimate that δ should be of the order 0.01. Such a large distortion of the high-energy tail would reduce the $p + p$ reaction rate by more than 20% (and other *pp*-chain reaction rates by an order of magnitude); as may be seen by considering Figure 6, such a large reduction in the $p + p$ reaction rate would not be compatible with the helioseismic sound speed profile. In addition, Bahcall et al. (2002) have criticized the above estimate of the magnitude δ

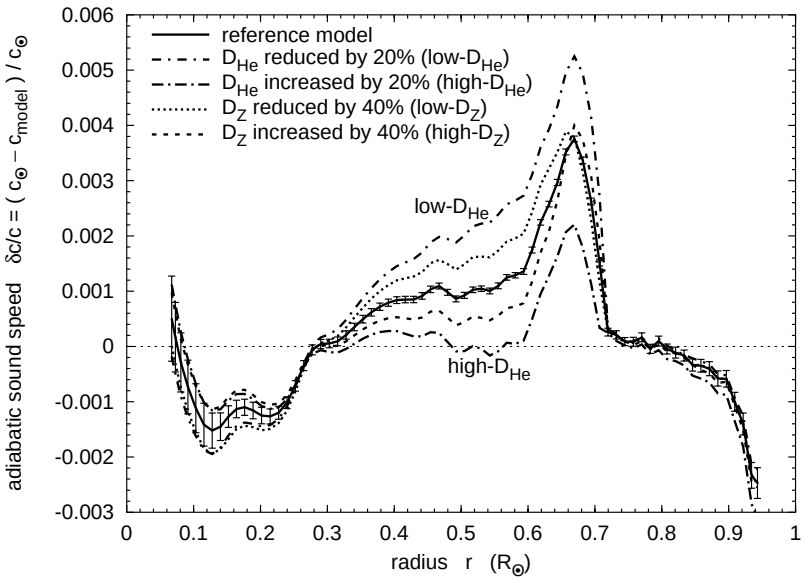

Fig. 7.— Effect on the sound speed of uncertainties in diffusion constants. The tested cases of a 20% variation in the diffusion constant for helium (*dot-dashed lines*) may overestimate that uncertainty slightly; on the other hand, the tested cases of a 40% variation in the heavy element diffusion constants (*dotted* and *short-dashed lines*) may slightly underestimate the corresponding uncertainties — the reference standard solar model is shown by the *solid line*.

of the effect, claiming that it should be negligibly small. Nonetheless, Turck-Chièze et al. (2001b) have considered the effect of such a Maxwellian distortion, with a smaller value of $\delta = 0.002$ — this reduces the $p + p$ reaction rate by only 5%, yielding a solar model whose sound speed differs by $\delta c/c \lesssim 0.005$ from the helioseismic profile (i.e., disfavored by helioseismology, but perhaps not ruled out entirely).

Diffusion effects: There are uncertainties in the diffusion coefficients; Proffitt (1994) estimates a 15% uncertainty in the diffusion constant of helium relative to hydrogen, and a $\sim 50\%$ uncertainty in the diffusion constant for oxygen relative to hydrogen. Figure 7 shows that an increase or decrease of 20% in the helium diffusion constants has only a modest effect: a maximum change of 0.001 in the sound speed, with $\mathrm{rms}\{\Delta c/c\} \approx 0.0008$ and $\mathrm{rms}\{\Delta\rho/\rho\} \approx 0.007$. The effect of increasing or decreasing the heavy element diffusion constants by 40% has a slightly smaller effect: a maximum change of 0.0006 in the sound speed, with $\mathrm{rms}\{\Delta c/c\} \approx 0.0004$ and $\mathrm{rms}\{\Delta\rho/\rho\} \approx 0.004$. Note that including the effects of different diffusion rates for different heavy elements would have an effect less than half as large as this, as shown by the results of Turcotte & Christensen-Dalsgaard (1998) and Turcotte et al. (1998).

3.2. Solar Convective Envelope Depth

One of the key results of helioseismic observations is a highly precise value for the position R_{ce} of the base of the solar surface convective region: Basu & Antia (1997) report a value of $R_{ce} = 0.713 \pm 0.001\ R_\odot$. Our reference standard solar model is in agreement with this value, having $R_{ce} = 0.7135\ R_\odot$ (see Table 1), with

values negligibly different ($R_{ce} = 0.7133$ or $0.7134\ R_\odot$) if we used the OPAL instead of the MHD equation of state at $\log \rho \lesssim -2$. The new Grevesse & Sauval (1998) solar abundance observations (implying $Z/X = 0.023$) yield a barely-consistent value of $R_{ce} = 0.7157\ R_\odot$; the maximum allowed abundance variations about this value (i.e., low and high Z/X values of 0.0203 and 0.0277, respectively) are inconsistent with the observed value (yielding $R_{ce} = 0.7209$ and $0.7098\ R_\odot$, respectively). The solar age uncertainty of ± 0.02 Gyr does not make a significant difference in R_{ce} (see Table 1). As far as the uncertainties in the nuclear reaction rates are concerned, only the *pp* rate has a significant effect on R_{ce}, of $\pm 0.002\ R_\odot$. Uncertainties in molecular opacities do not have a significant effect on R_{ce}, but changing from the old 1985 LAOL opacities to the 1995 OPAL opacities does yield a large improvement (of $0.006\ R_\odot$); the remaining uncertainties in the 1995 OPAL opacities might thus be expected to have a small but possibly significant effect on R_{ce}. The uncertainty in the diffusion constant for helium does have a significant influence ($\pm 0.003\ R_\odot$), but uncertainties in the diffusion constants for the heavy elements do not (effects $\lesssim 0.001\ R_\odot$).

Note that the cases favored by the sound speed profiles at the one- to two-sigma significance level (high opacities, high Z/X, or high *pp* rate) are disfavored by the observed R_{ce} value at about the same significance level.

3.3. Solar Helium Abundance

Another key result of helioseismic observations is a fairly precise value for the present solar envelope helium mass fraction Y_e (this value is lower than the Sun's initial helium abundance, due to diffusion). Inferring the solar helium abundance requires the use of a (theoretical) equation of state, as well as helioseismic frequency observations of modes that probe the solar convective region, particularly the He II ionization zone (Richard et al. 1998).

Table 2 quotes helioseismic Y_e values from eight recent papers — note that most authors calculate two separate values, obtained using the OPAL and MHD equations of state, respectively. Clearly, the systematic errors are much larger than the quoted internal errors from the helioseismic inversions, as shown by the relatively large differences between values obtained with these two different equations of state, and by the differences between determinations by different investigators. The OPAL equation of state is expected to be more accurate than the MHD equation of state over the bulk of the convective envelope, since the MHD equation of state was designed for use at $\log \rho \lesssim -2$ (which occurs in the Sun at $r \gtrsim 0.942\ R_\odot$); however, the He II ionization zone occurs further out ($0.975\ R_\odot \lesssim r \lesssim 0.985\ R_\odot$) in a region the MHD equation of state was specifically designed for, and where it may actually be more accurate than the OPAL equation of state (see, e.g., Richard et al. 1998; Basu et al. 1999; Di Mauro et al. 2002). Possible reasons for the relatively large scatter among Y_e values of different investigators (even when using the same equation of state) are discussed by Di Mauro et al. (2002); they point out that observational frequencies for high-degree oscillation modes may suffer from significant systematic errors, and that the inversion formulae used to obtain Y_e ignore several physical effects that may significantly affect the frequencies in this region of the Sun, such as nonadiabaticity, effects of mode excitations, or flows resulting from convective turbulence — certainly there is evidence that turbulent motions affect the f-modes (Gough 1993; Chitre, Christensen-Dalsgaard, & Thompson 1998; Murawski, Duvall, & Kosovichev 1998; Mędrek, Murawski, & Roberts 1999; Di Mauro et al. 2002).

One may perhaps ignore the extremely low value of $Y_e \approx 0.226$ of Shibahashi, Hiremath, & Takata (1999), since it was obtained not from a direct inversion but by fitting to a sound speed profile (that had in

turn been obtained via a helioseismic inversion); relatively poor accuracy for this method is also suggested by the fact that the simultaneous determination by these authors of the depth of the solar convective envelope yielded $R_{ce} \approx 0.718\ R_\odot$, quite far from helioseismic value of $R_{ce} = 0.713 \pm 0.001\ R_\odot$ (Basu & Antia 1997). The remaining Y_e values from Table 2 have a mean of 0.245, a median value of 0.248, and a total range of $0.23 \leq Y_e \leq 0.254$, with most of the values lying in the range $0.24 \lesssim Y_e \lesssim 0.25$. These results can be conveniently summarized as an "observed" value of $Y_e = 0.245 \pm 0.005$ (where most of the uncertainty is due to systematic effects).

Our theoretical reference standard solar model is in excellent agreement with this, having $Y_e = 0.2424$ independent of whether we used the OPAL or the MHD equation of state at $\log \rho \lesssim -2$. Low and high Z/X values (0.0203 and 0.0277, respectively) yield Y_e values of 0.2396 and 0.2510, respectively — still quite acceptable. Similarly acceptable changes of ± 0.005 in Y_e result from a 4% uncertainty in the opacities, a 15% uncertainty in helium diffusion constants, or a 50% uncertainty in heavy-element diffusion constants. Uncertainties in the solar age, luminosity, and radius and in the nuclear rates have only a negligible effect on Y_e (see Table 1).

3.4. Solar Lithium Abundance

The present observed solar surface lithium abundance is $\log \varepsilon(^7\mathrm{Li}) = 1.10 \pm 0.10$ as compared to the initial value of $\log \varepsilon(^7\mathrm{Li}) = 3.31 \pm 0.04$ obtained from meteorites (Grevesse & Sauval 1998), where $\log \varepsilon(^7\mathrm{Li}) = \log(N_{\mathrm{Li}}/N_{\mathrm{H}}) + 12$ for number densities N_{Li} and N_{H} of lithium and hydrogen, respectively. The solar surface lithium depletion factor f_{Li}, relative to its initial value, is thus observed to be $f_{\mathrm{Li}} = 160 \pm 40$. Solar surface lithium can be depleted due to three causes: (1) lithium burning during the pre-main-sequence evolution, when the surface convection still reaches deeply into the interior; (2) rotationally induced mixing on the main sequence, which transports lithium down from the convective envelope to regions hot enough for lithium burning; (3) mass loss on the main sequence, which can cause the convective envelope to move inwards and engulf lithium-depleted regions. In this paper, we only consider the first of these, namely, the pre-main-sequence lithium destruction; rotational mixing is beyond the scope of this paper, and main sequence mass loss is discussed in the companion "Our Sun V" paper (Sackmann & Boothroyd 2002). Our reference standard solar model had a pre-main-sequence lithium depletion factor $f_{\mathrm{Li}} = 24$, as shown in Table 1. This is a relatively large pre-main-sequence lithium depletion, leaving only a factor of ~ 7 to be accounted for by main sequence effects (2) and (3) above. Note that the recent models of Brun et al. (1999) also appear to find solar pre-main-sequence lithium depletion by a factor of order 10 (in good agreement with our results, considering the sensitivity of pre-main-sequence lithium depletion to the input physics).

It is worth noting that, in the past, pre-main-sequence lithium depletion in the Sun has often been ignored or assumed to be negligible (which is not the case, as our present models show). Earlier models did in fact show relatively little pre-main-sequence solar lithium depletion, e.g., a depletion factor of 3 was reported by Sackmann et al. (1993). These low lithium depletion factors may have been caused partly by the use of older opacity tables in earlier models, but a major contributing factor was neglect of gravitational settling (diffusion) of helium and the heavy elements. These earlier models thus had a lower metallicity during the pre-main-sequence stage, matching the present solar surface metallicity, rather than being about 10% higher (as diffusion models indicate). Because of the strong metallicity dependence of pre-main-sequence lithium depletion, such models yielded relatively small depletion factors.

Pre-main-sequence lithium depletion depends quite sensitively on the structure of the solar models during

that stage of evolution. We give our results in terms of the solar lithium depletion factor $f_{\rm Li}$, which is shown in Table 1. The zoning did not affect the lithium depletion factor significantly; nor did the uncertainties in the solar age, luminosity, and radius. Changes in the equation of state in the outermost regions can have a small effect ($\lesssim 30\%$) on the lithium depletion factor: the "OPALeos-midT" and "OPALeos-lowT" cases had lithium depletion factors of $f_{\rm Li} = 17$ and 19, respectively, as opposed to $f_{\rm Li} = 24$ for the standard "OPALeos-hiT" case.

The pre-main-sequence lithium depletion is extremely sensitive to both low-temperature and high-temperature opacities; use of the Sharp (1992) molecular opacities instead of the Alexander & Ferguson (1994) ones halved the lithium depletion factor ($f_{\rm Li} = 10$), as did our "low-κ" test case ($f_{\rm Li} = 10$), while our "high-κ" test case nearly tripled it ($f_{\rm Li} = 71$). There is also a relatively large sensitivity to the uncertainty in the observed solar abundances. A low Z/X ratio of 0.0203 (with "$\kappa_{\rm OPAL:GS98\downarrow C-Ne}$") yields only two-thirds as much lithium depletion ($f_{\rm Li} = 15$), while a high Z/X ratio of 0.0257 (with "$\kappa_{\rm OPAL:GS98\uparrow C-Ne}$") yields half again as much lithium depletion ($f_{\rm Li} = 35$).

Uncertainties in the diffusion constants can affect the lithium depletion factor significantly, primarily due to the effect of the different initial composition; our diffusion test cases have depletion factors ranging from $f_{\rm Li} = 18$ to 33.

Except for the $^7{\rm Li} + p$ rate, uncertainties in the nuclear rates have almost no effect on the extent of lithium depletion. For the $^7{\rm Li} + p$ rate, the $\pm 14\%$ uncertainty quoted by the NACRE compilation (Angulo et al. 1999) corresponds to an uncertainty of about $\pm 50\%$ in the depletion factor (i.e., a range in the from $f_{\rm Li} = 16$ to 38).

Solar beryllium abundance: The observed solar beryllium abundance is $\log \varepsilon(^9{\rm Be}) = 1.40 \pm 0.09$, consistent with no depletion relative to the meteoritic value of $\log \varepsilon(^9{\rm Be}) = 1.42 \pm 0.04$. The quoted uncertainties of these values imply that solar beryllium cannot have been depleted by more than a factor of 2 (3-σ upper limit). Our solar models all have negligible amounts of beryllium depletion, of order 1% — in good agreement with these observational beryllium results. Other authors have shown that parameterized rotational-mixing models which match the observed solar lithium depletion yield relatively minor beryllium depletion, in agreement with observations. For example, the rotational-mixing solar models of Brun et al. (1999), with total lithium depletion of a factor of order 100 (a factor of ~ 10 occurring on the main sequence), deplete beryllium by only about 12%. Note that rotational-mixing models which ignore pre-main-sequence lithium depletion (i.e., which over-estimate the main-sequence lithium depletion by an order of magnitude) might be expected to overestimate the beryllium depletion as well: for example, Richard et al. (1996) required main-sequence lithium depletion by a factor of 155 in their solar models with rotational mixing, and found that these models then implied beryllium depletion by a factor of 2.9.

3.5. Solar neutrinos

We will not devote much space to the predicted solar neutrino values, since it has long been concluded that matching the observed neutrino capture rates requires not revised astrophysics but new neutrino physics, e.g., Mikheyev-Smirnov-Wolfenstein (MSW) neutrino oscillation effects — even non-standard solar models (e.g., with core mixing or a low-metallicity core) cannot simultaneously satisfy the neutrino observations and the helioseismic constraints (see, e.g., Bahcall, Basu, & Pinsonneault 1998a; Suzuki 1998; Basu et al. 2000; Bahcall et al. 2001; Watanabe & Shibahashi 2001; Turck-Chièze et al. 2001a,b; Choubey et al. 2001; Guzik

et al. 2001). In Table 1 we present the theoretically predicted neutrino capture rates for the ^{37}Cl and ^{71}Ga experiments, and the predicted flux of ^{8}B neutrinos. As is normally obtained, our theoretical predicted neutrino rates are much in excess of the observed values, i.e., 6.4 to 8.9 SNU is predicted for the ^{37}Cl experiment, as compared to the observed value of 2.56 ± 0.23 SNU (Davis 1994; Cleveland et al. 1998), and 127 to 141 SNU for the ^{71}Ga experiments, as compared to the observed value of 74.5 ± 5.7 SNU (combined value from SAGE and GALLEX+GNO: Hampel et al. 1999; Abdurashitov et al. 1999; Altmann et al. 1999; Gavrin 2001; Ferrari 2001). Likewise, the models predict ^{8}B neutrino fluxes of 4.4 to 6.3×10^6 cm^{-2} s^{-1}, as compared to the value of $(2.32 \pm 0.08) \times 10^6$ cm^{-2} s^{-1} implied by the Super-Kamiokande measurement (Fukuda et al. 2001).

4. Conclusion

Helioseismic frequency observations enable the adiabatic sound speed c and adiabatic index Γ_1 to be inferred with an accuracy of a few parts in 10^4, and the density ρ with an accuracy of a few parts in 10^3. These quantities can also be computed on purely theoretical grounds. It is important to understand the uncertainties in these theoretical quantities (arising from uncertainties in the input data), when comparing them to the values inferred from helioseismic measurements. These uncertainties in the theoretical standard solar model are presented below.

(1) Abundances of the elements: For the standard solar model, we found that the largest impact on the sound speed arises from the observational uncertainties in the photospheric abundances of the elements. The key elements for which accurate meteoritic determinations are not available are C, N, O, and Ne, with uncertainties of 15% (leading to an uncertainty of order 10% in the solar Z/X ratio). We determined that this abundance uncertainty affects the sound speed profile in the solar model at the level of 3 parts in 10^3.

(2) OPAL opacities, *pp* nuclear rate, and diffusion constants: The estimated 4% uncertainty in the OPAL opacities, the $\sim 5\%$ uncertainty in the basic *pp* nuclear reaction rate, the $\sim 15\%$ uncertainty in the diffusion constants for the gravitational settling of helium, and the $\sim 50\%$ uncertainties in diffusion constants for the heavier elements, all affect the sound speed at the level of 1 part in 10^3.

(3) Solar radius and low-temperature equation of state: Different observational methods yield values for the solar radius differing by as much as 7 parts in 10^4; this leads to uncertainties of a few parts in 10^3 in the sound speed in the solar convective envelope, but has negligible effect on the interior (recall, however, that while the sound speed in the solar model is not affected, there is a systematic effect on the "observed" *helioseismic* sound speed profile). Uncertainties in the low-temperature equation of state ($\log T \lesssim 5.5$) lead to uncertainties of order a part in 10^3 in both the sound speed and the adiabatic index Γ_1 in the convective envelope.

(4) Rotational mixing and high-temperature equation of state: We did not explicitly consider the effects of rotational mixing or uncertainties in the interior equation of state, but other investigators have found these to yield uncertainties in the sound speed of order a part in 10^3, as discussed in § 3.1.

(5) Other sources of uncertainty: We found that other current uncertainties, namely, in the solar age and luminosity, in nuclear rates other than the *pp* reaction and in the low-temperature molecular opacities, have no significant effect on the quantities that can be inferred from helioseismic observations (although some of these can have significant effects on neutrino fluxes and/or the extent of pre-main-sequence lithium depletion).

(6) Depth of envelope convection: Our reference standard solar model (with $Z/X = 0.0245$) yielded a convective envelope position $R_{ce} = 0.7135\ R_\odot$, in excellent agreement with the observed value of $0.713 \pm 0.001\ R_\odot$, and was significantly affected ($\pm 0.003\ R_\odot$) only by uncertainties in Z/X, opacities, the *pp* rate, and helium diffusion constants.

(7) Envelope helium abundance: Our reference model yielded an envelope helium abundance $Y_e = 0.2424$, in good agreement with the range of values inferred from helioseismic observations (which we summarize as a helioseismic $Y_e = 0.245 \pm 0.005$); only extreme variations in Z/X, opacities, or diffusion constants yielded Y_e variations as large as 0.005.

(8) Pre-main-sequence lithium depletion: For the standard solar model, the predicted pre-main-sequence lithium depletion is a factor of order 20 (an order of magnitude larger than that predicted by earlier models that neglected gravitational settling and used older opacities). The lithium depletion factor can vary between ~ 10 and ~ 40 when one varies the input physics, i.e., it is uncertain by a factor of 2.

(9) Solar neutrinos: For the standard solar model, the predicted neutrino capture rate is uncertain by $\sim 30\%$ for the ^{37}Cl experiment and by $\sim 3\%$ for the ^{71}Ga experiments (not including uncertainties in the capture cross sections), while the ^{8}B neutrino flux is uncertain by $\sim 30\%$.

We are indebted to Prof. Marc H. Pinsonneault for helpful discussions on diffusion and for providing us with his diffusion code. We are grateful to Prof. Sarbani Basu for discussions of helioseismology, and for providing us with the current helioseismic reference model; we are also grateful to Prof. Dimitri M. Mihalas, for providing us with his equation-of-state code. We wish to thank Prof. Charles A. Barnes and Prof. Yuk L. Yung for thoughtful discussions and encouragement. We wish to acknowledge the support provided by Prof. Thomas A. Tombrello, Chairman of the Division of Physics, Math, and Astronomy, and Prof. Robert D. McKeown, Head of the W. K. Kellogg Radiation Laboratory. One of us (I.-J. S.) wishes to thank Alexandra R. Christy, her daughter, and Prof. Robert F. Christy, her husband, for their supportiveness, and Robert F. Christy for critical analysis and helpful comments. One of us (A. I. B.) wishes to thank Prof. Peter G. Martin and Prof. J. Richard Bond for their support, and M. Elaine Boothroyd, his wife, for her patience and encouragement. This work was supported by a grant NAG5-7166 from the Sun-Earth Connection Program of the Supporting Research and Technology and Suborbital Program in Solar Physics of the National Aeronautics and Space Administration, and by the National Science Foundation grant NSF-0071856 to the Kellogg Radiation Laboratory.

REFERENCES

Abdurashitov, J.N. et al. 1999, Phys. Rev. Lett., 83, 4686 (GALLEX Collaboration)

Alexander, D. R., & Ferguson, J. W. 1994, ApJ, 437, 879

Altmann, M., et al. 1999, Phys. Lett. B, 490, 16 (GNO Collaboration)

Anders, E., & Grevesse, N. 1989, Geochim. Cosmochim. Acta, 53, 197

Angulo, C. et al. 1999, Nucl. Phys. A, 656, 3

Antia, H. M. 1998, A&A, 330, 336

Antia, H. M., & Chitre, S. M. 1999, A&A, 347, 1000

Aufderheide, M. B., Bloom, S. B., Resler, D. A., & Goodman, C. D. 1994, Phys. Rev. C, 49, 678

Bahcall, J. N., Bahcall, N. A., & Shaviv, G. 1968, Phys. Rev. Lett., 20, 1209

Bahcall, J. N., Basu, S., & Pinsonneault, M.H. 1998a, Phys. Lett. B, 433, 1

Bahcall, J. N., Brown, L. S., Gruzinov, A., & Sawyer, R. F. 2002, A&A, 383, 291; —. 2002, A&A, 388, 660 (Erratum)

Bahcall, J. N., Chen, X. L., & Kamionkowski, M. 1998b, Phys. Rev. C, 57, 2756

Bahcall, J. N., & Moeller, C. P. 1969, ApJ, 155, 511

Bahcall, J. N., Pinsonneault, M. H., & Basu, S. 2001, ApJ, 555, 990

Bahcall, J. N., Pinsonneault, M. H., & Wasserburg, G. J. 1995, Rev. Mod. Phys., 67, 781

Bahcall, J. N., & Ulrich, R. K. 1988, Rev. Mod. Phys., 60, 297

Basu, S. 1998, MNRAS, 298, 719

Basu, S., & Antia H. M. 1995, MNRAS, 276, 1402

Basu, S., & Antia H. M. 1997, MNRAS, 287, 189

Basu, S., Däppen, W., & Nayfonov, A. 1999, ApJ, 518, 985

Basu, S., Pinsonneault, M. H., & Bahcall, J. N. 2000, ApJ, 529, 1084

Baturin, V. A., & Ayukov, S. V. 1997, in SCORe '96: Solar Convection and Oscillations and their Relationship, ed. F. P. Pijpers, J. Christensen-Dalsgaard, & C. Rosenthal (Dordrecht: Kluwer), 55

Boothroyd, A. I., & Sackmann, I.-J. 1999, ApJ, 510, 232

Brown, T. M., & Christensen-Dalsgaard, J. 1998, ApJ, 500, L195

Brown, L. S., & Sawyer, R. F. 1997, Rev. Mod. Phys., 69, 411

Brüggen, M., & Gough, D. O. 1997, ApJ, 488, 867

Brun, A. S., Turck-Chièze, S., & Zahn, J. P. 1999, ApJ, 525, 1032

Carraro, C., Schäfer, A., & Koonin, S. E. 1988, ApJ, 331, 565

Caughlan, G. R., & Fowler, W. A. 1988, Atomic Data Nucl. Data Tables, 40, 283

Chaplin, W. J., Elsworth, Y., Howe, R., Isaak, G. R., McLeod, C. P., Miller, B. A., van der Raay, H. B., Wheeler, S. J., & New, R. 1996, Sol. Phys., 168, 1

Chitre, S. M., Christensen-Dalsgaard, J., & Thompson, M. J. 1998, in Structures and Dynamics of the Interior of the Sun and Sun-like Stars, Proc. SOHO 6/GONG 98 Workshop, ed. S. G. Korzennik & A. Wilson, ESA SP-418 (Noordwijk, The Netherlands: ESA Publications Division), 141

Choubey, S., Goswami, S., Kar, K., Antia, H. M., & Chitre, S. M. 2001, Phys. Rev. D, 64, 113001

Christensen-Dalsgaard, J., & Däppen, W. 1992, A&A Rev., 4, 267

Cleveland, B. T., Daily, T., Davis, R., Jr., Distel, J. R., Lande, K., Lee, C. K., Wildenhain, P. S., & Ullman, J. 1998, ApJ, 496, 505

Cohen, E. R., & Taylor, B. N. 1986, Codata Bulletin No. 63 (New York: Pergamon)

Coraddu, M., Kaniadakis, G., Lavagno, A., Lissia, M., Mezzorani, G., & Quarati, P. 1999, Brazilian J. Phys., 29, 153

Crommelynck, D., Fichot, A., Domingo, V., & Lee, R. 1996, Geophys. Res. Lett., 23, 2293

Däppen, W., Gough, D. O., Kosovichev, A. G., & Rhodes, E. J., Jr. 1993, in IAU Symp. 137, Inside the Stars, ed. W. Weiss & A. Baglin (San Francisco: PASP), 304

Däppen, W., Mihalas, D., Hummer, D. G., & Mihalas, B. 1988, ApJ, 332, 261

Davis, R. 1994, Prog. Part. Nucl. Phys., 32, 13

Di Mauro, M. P., Christensen-Dalsgaard, J., Rabello-Soares, M. C., & Basu, S. 2002, A&A, 384, 666

Elliot, J. R., & Kosovichev, A. G. 1998, ApJ, 500, L199

Ferrari, N. 2001, Nucl. Phys. B, 100, 48

Fiorentini, G., Ricci, B., & Villante, F. L. 2001, Phys. Lett. B, 503, 121

Fröhlich, C., & Lean, J. 1998, Geophys. Res. Lett., 25, 4377

Fukuda,S., et al. 2001, Phys. Rev. Lett., 86, 5651 (Super-Kamiokande Collaboration)

Gabriel, M. 1997, A&A, 327, 771

Gavrin, V. N. 2001, Nucl. Phys. B, 91, 36

Geiss, J. 1973, in Proc. 13th Intl. Cosmic Ray Conf., vol. 5 (Denver: Univ. of Denver), 3375

Geiss, J., & Bochsler, P. 1991, in The Sun in Time, ed. C. Sonnett, M. Giampapa, & M. Matthews (Tucson: Univ. Arizona Press), 98

Gong, Z., Däppen, W., & Nayfonov, A. 2001, ApJ, 563, 419

Gong, Z., Däppen, W., & Zedja, L. 2001, ApJ, 546, 1178

Gough, D. O. 1993, in Astrophysical Fluid Dynamics, Les Houches Session XLVII, ed. J.-P. Zahn & J. Zinn-Justin (Amsterdam: Elsevier),399

Gough, D. O., Leibacher, J. W., Scherrer, P. H., & Toomre, J. 1996, Science, 272, 1281

Graboske, H. C., DeWitt, H. E., Grossman, A. S., & Cooper, M. S. 1973, ApJ, 181, 457

Grevesse, N. 1984, Phys. Scr, T8, 49

Grevesse, N., & Noels, A. 1993, in Origin and Evolution of the Elements, ed. N. Prantzos, E. Vangioni-Flam, & M. Cassé (Cambridge: Cambridge Univ. Press), 15

Grevesse, N., & Sauval, A. J. 1998, Space Sci. Rev., 85, 161

Gruzinov, A. V. 1998, ApJ, 496, 503

Gruzinov, A. V., & Bahcall, J. N. 1997, ApJ, 490, 437

Gruzinov, A. V., & Bahcall, J. N. 1998, ApJ, 504, 996

Guenther, D. B. 1989, ApJ, 339, 1156

Guenther, D. B., Demarque, P., Kim, Y.-C., & Pinsonneault, M. H. 1992, ApJ, 387, 372

Guzik, J. A., Neuforge-Verheecke, C., Young, A. C., Epstein, R. I., Poulin, F. M., & Schissel, J. R. 2001, Sol. Phys., 200, 305

Guzik, J. A., & Swenson, F. J. 1997, ApJ, 491, 967

Hampel, W., et al. 1999, Phys. Lett. B, 447, 127 (GALLEX Collaboration)

Harvey, J. W., et al. 1996, Science, 272, 1284

Iglesias, C. A., & Rogers, F. J. 1996, ApJ, 464, 943

Itoh, N., Totsuji, H., Ichimaru, S., & DeWitt, H. E. 1979, ApJ, 234, 1079; —. 1979, ApJ, 239, 415 (Erratum)

Ichimaru, S., & Utsumi, K. 1983, ApJ, 269, L51

Kerridge, J. F., Signer, P., Wieler, R., Becker, R. H., & Pepin, R. O. 1991, in The Sun in Time, ed. C. Sonnett, M. Giampapa, & M. Matthews (Tucson: Univ. Arizona Press), 389

Kosovichev, A. G. 1997, in AIP Conf. Proc. 385, Robotic Exploration Close to the Sun: Scientific Basis, ed. S. R. Habbal (Woodbury, NY: Amer. Inst. Phys.), 159

Lean, J. 2000, Geophys. Res. Lett., 27, 2425

Magee, N. H. et al. 1995, in ASP Conf. Ser. 78, Proc. Joint Discussion 16 of the 22nd General IAU Assembly, Astrophysical Applications of Powerful New Databases, Ed. S. J. Adelman & W. L. Wiese (San Francisco: ASP), 51

Mędrek, M., Murawski, K., & Roberts, B. 1999, A&A, 349, 312

Morel, P., Provost, J., & Berthomieu, G. 1997, A&A, 327, 349

Murawski, K., Duvall, T. L., & Kosovichev, A. G. 1998 in Structures and Dynamics of the Interior of the Sun and Sun-like Stars, Proc. SOHO 6/GONG 98 Workshop, ed. S. G. Korzennik & A. Wilson, ESA SP-418 (Noordwijk, The Netherlands: ESA Publications Division), 825

Neuforge-Verheecke, C., Goriely, S., Guzik, J. A., Swenson, F. J., & Bradley, P. A. 2001a, ApJ, 550, 493

Neuforge-Verheecke, C., Guzik, J. A., Keady, J. J., Magee, N. H., Bradley, P. A., & Noels, A. 2001b, ApJ, 561, 450

Pérez Hernández, F., & Christensen-Dalsgaard, J. 1994, MNRAS, 269, 475

Proffitt, C. R. 1994, ApJ, 425, 849

Rhodes, E. J., Jr., Kosovichev, A. G., Schou, J., Scherrer, P. H., & Reiter, J. 1997, Sol. Phys., 175, 287

Richard, O., Dziembowski, W. A., Sienkiewicz, R., & Goode, P. R. 1998, A&A, 338, 756

Richard, O., Vauclair, S., Charbonnel, C., & Dziembowski, W. A. 1996, ApJ, 312, 1000

Rogers, F. J. 2000, Physics of Plasmas, 7, 51

Rogers, F. J. 2001, Contributions to Plasma Physics, 2001, 41, 179

Rogers, F. J., & Iglesias, C. A. 1992, ApJS, 79, 507

Rogers, F. J., & Iglesias, C. A. 1992, Space Sci. Rev., 85, 61

Rogers, F. J., Swenson, F. J., & Iglesias, C. A. 1996, ApJ, 456, 902

Sackmann, I.-J., & Boothroyd, A. I. 2001, ApJ, in press (Our Sun V)

Sackmann, I.-J., Boothroyd, A. I., & Kraemer, K. E. 1993, ApJ, 418, 457

Salpeter, E. E. 1955, ApJ, 121, 161

Sharp, C. M. 1992, A&AS, 94, 1

Shaviv, G., & Shaviv, N. J. 2000, ApJ, 529, 1054

Shaviv, N. J., & Shaviv, G. 1996, ApJ, 468, 433

Shaviv, N. J., & Shaviv, G. 2001, ApJ, 558, 925

Shibahashi, H., Hiremath, K. M., & Takata, M. 1999, Adv. Space Sci., 24, 177

Suzuki, Y. 1998, Space Sci. Rev., 85, 91

Thoul, A. A., Bahcall, J. N., & Loeb, A. 1994, ApJ, 421, 828

Tomczyk, S., Streander, K., Card, G., Elmore, D., Hull, H., & Caccani, A. 1995, Sol. Phys., 159, 1

Tsytovich, V. N. 2000, A&A, 356, L57

Tsytovich, V. N., & Bornatici, M. 2000, Plasma Phys. Rep., 26, 840

Turck-Chièze, S., et al. 2001a, ApJ, 555, L69

Turck-Chièze, S., Nghiem, P, Couvidat, S., & Turcotte, S. 2001b, Sol. Phys., 200, 323

Turcotte, S., & Christensen-Dalsgaard, J. 1998, Space Sci. Rev. 85, 133

Turcotte, S., Richer, J., Michaud, G., Iglesias, C. A., & Rogers, F. J. 1998, ApJ, 504, 539

Ulrich, R. K., & Rhodes, E. R., Jr. 1983, ApJ, 265, 551

Wasson, J. T. 1985, Meteorites: Their Record of Early Solar-System History (New York: Freeman)

Watanabe, S., & Shibahashi, H. 2001, PASJ, 53, 565

Weiss, A., Flaskamp, M., & Tsytovich, V. N. 2001, A&A, 371, 1123

Wood, B. E., Müller, H.-R., Zank, G. P., & Linsky, J. L. 2002, ApJ, 574, 412

Table 1. Characteristics of Our Solar Models[a]

Solar Model	α	Z_0	Y_0	Y_e	R_{ce} ($R_\odot$)	rms $\delta c/c$ for: all-r	rms $\delta c/c$ for: < 0.6	rms $\delta\rho/\rho$	relative rms vs.	relative rms $\Delta c/c$	relative rms $\Delta\rho/\rho$	$f_{\rm Li}$	$\Phi_{\rm Cl}$	$\Phi_{\rm Ga}$	$\Phi_{\rm B}$
1. Fine-zoned Reference[b]	1.817	.02030	.2760	.2424	.7135	.00133	.00085	.01698		...	...	24.24	7.87	133.7	5.31
2. Fine-zoned, OPALeos-midT[c]	1.803	.02031	.2760	.2424	.7133	.00131	.00085	.01716	1	.00029	.00054	19.08	7.87	133.7	5.31
3. Fine-zoned, OPALeos-lowT[d]	1.814	.02031	.2760	.2424	.7134	.00132	.00085	.01709	1	.00013	.00026	16.81	7.87	133.8	5.32
4. Coarse-zoned Reference[b,e]	1.814	.02030	.2760	.2424	.7136	.00140	.00091	.01772	1[f]	.00008	.00074	24.36	7.89	133.8	5.33
5. OPALeos-midT[c]	1.800	.02029	.2760	.2425	.7135	.00139	.00092	.01807	2[f]	.00010	.00092	19.74	7.90	134.0	5.34
6. $R_\odot = 695.78$ Mm (R78)	1.815	.02027	.2760	.2427	.7134	.00134	.00089	.01880	4	.00045	.00151	24.22	7.95	134.3	5.38
7. $R_\odot = 695.508$ Mm (R508)	1.819	.02028	.2760	.2425	.7129	.00130	.00092	.01933	4	.00098	.00256	24.70	7.90	134.0	5.34
8. R78, OPALeos-midT	1.803	.02030	.2760	.2424	.7131	.00136	.00085	.01851	5[g]	.00041	.00097	19.95	7.89	133.8	5.33
9. R508, OPALeos-midT	1.804	.02027	.2759	.2427	.7129	.00148	.00093	.02001	5[g]	.00099	.00276	19.84	7.95	134.3	5.38
10. $L_\odot = L_{best}$[h]	1.808	.02029	.2757	.2421	.7137	.00143	.00092	.01739	4	.00012	.00053	23.95	7.73	132.8	5.21
11. $L_\odot = L_{best} - 0.8\%$ (L_{low})	1.794	.02030	.2749	.2416	.7138	.00145	.00094	.01681	10[g]	.00015	.00107	23.39	7.38	130.3	4.94
12. $L_\odot = L_{best} + 0.8\%$ (L_{high})	1.823	.02028	.2765	.2429	.7135	.00140	.00093	.01839	10[g]	.00014	.00133	24.62	8.16	135.7	5.54
13. $t_\odot = 4.5$ Gyr	1.801	.02022	.2768	.2436	.7149	.00195	.00148	.02374	4	.00064	.00609	21.75	7.73	133.1	5.22
14. $t_\odot = 4.7$ Gyr	1.826	.02034	.2752	.2415	.7124	.00099	.00057	.01253	4	.00056	.00528	26.82	8.03	135.2	5.51
15. $Z_\kappa = Z_h$, CNO-interpolation	1.813	.02030	.2762	.2425	.7137	.00144	.00095	.01818	4	.00006	.00047	24.16	7.90	134.0	5.36
16. $Z_\kappa = Z_h$, $CO_{ex} = 0.0$[i]	1.815	.02030	.2759	.2424	.7134	.00135	.00088	.01735	4	.00007	.00039	24.55	7.86	133.7	5.30
17. $Z_\kappa = Z_0$ (const-Z_κ)	1.823	.02026	.2759	.2430	.7073	.00068	.00046	.01137	4	.00098	.00685	24.96	7.72	133.1	5.20
18. $Z_\kappa = Z_0$, $CO_{ex} = Z - Z_\kappa$	1.820	.02027	.2760	.2428	.7105	.00092	.00052	.01364	4	.00059	.00428	24.71	7.79	133.5	5.25
19. $Z_\kappa = Z$ (approx-κ)	1.812	.02030	.2764	.2427	.7138	.00151	.00103	.01898	4	.00016	.00131	23.86	8.00	134.4	5.42
20. $Z_\kappa = 0.9\,Z$ (low-κ)	1.824	.02056	.2659	.2331	.7178	.00313	.00266	.03376	4	.00184	.01619	9.72	7.08	129.8	4.70
21. $Z_\kappa = 0.95\,Z$	1.819	.02044	.2713	.2379	.7156	.00225	.00178	.02591	4	.00094	.00830	14.95	7.50	131.9	5.04
22. $Z_\kappa = 1.05\,Z$	1.805	.02016	.2813	.2474	.7121	.00094	.00045	.01315	4	.00063	.00471	39.97	8.58	137.4	5.87
23. $Z_\kappa = 1.1\,Z$ (high-κ)	1.797	.02003	.2860	.2516	.7106	.00069	.00055	.00689	4	.00126	.01148	70.62	9.04	139.6	6.24
24. $\kappa_{\rm LOAL85}$ at high T	1.882	.02051	.2688	.2356	.7193	.00485	.00380	.03862	4	.00359	.02179	11.82	7.24	130.7	4.83
25. $\kappa_{\rm Sharp}$ at low T	1.762	.02027	.2759	.2426	.7137	.00144	.00096	.01820	4	.00006	.00050	12.06	7.94	134.2	5.37
26. $\kappa_{\rm OPAL:GN93\uparrow C-Ne}$ (unmatched)[j]	1.834	.02045	.2679	.2356	.7132	.00159	.00143	.02330	4	.00048	.00565	15.12	7.03	130.2	4.74
27. $\kappa_{\rm OPAL:GN93\downarrow C-Ne}$ (unmatched)[j]	1.791	.02009	.2851	.2504	.7142	.00140	.00056	.01219	4	.00051	.00572	46.66	8.91	138.8	6.14
28. $Z/X = .023$ (unmatched κ)[j]	1.795	.01923	.2712	.2376	.7158	.00227	.00182	.02653	4	.00096	.00891	15.16	7.29	130.5	4.89
29. $Z/X = .023$, $\kappa_{\rm OPAL:GS98}$	1.787	.01911	.2758	.2419	.7157	.00192	.00122	.02125	4	.00056	.00374	22.60	7.76	132.8	5.26
30. $Z/X = .0257$, $\kappa_{\rm OPAL:GS98\uparrow C-Ne}$	1.840	.02121	.2768	.2438	.7113	.00072	.00046	.01079	29[g]	.00152	.01115	35.00	8.07	135.2	5.46
31. $Z/X = .0203$, $\kappa_{\rm OPAL:GS98\downarrow C-Ne}$	1.728	.01700	.2749	.2396	.7209	.00366	.00267	.03375	29[g]	.00180	.01276	14.81	7.41	130.2	5.04
32. $Z/X = .0277$ (unmatched κ)[j]	1.851	.02251	.2853	.2517	.7094	.00091	.00100	.00315	4	.00176	.01704	77.94	9.20	141.3	6.30
33. $Z/X = .0277$, $\kappa_{\rm OPAL:Gr84}$	1.845	.02255	.2848	.2510	.7098	.00076	.00077	.00851	4	.00139	.01095	52.25	9.87	145.6	6.76
34. high pp rate	1.841	.02014	.2772	.2447	.7108	.00074	.00065	.01042	4	.00136	.02614	24.20	6.61	127.2	4.37
35. low pp rate	1.805	.02035	.2756	.2417	.7146	.00185	.00141	.02683	4	.00051	.00936	24.32	8.44	136.7	5.75
36. high ^{3}He + α rate	1.817	.02026	.2763	.2430	.7132	.00127	.00078	.01452	4	.00018	.00349	24.03	8.84	140.1	6.04
37. low ^{3}He + α rate	1.810	.02031	.2757	.2421	.7140	.00157	.00111	.02186	4	.00021	.00432	24.43	6.91	127.7	4.60
38. high ^{3}He + ^{3}He rate	1.813	.02028	.2759	.2425	.7137	.00146	.00098	.01883	4	.00008	.00115	24.06	7.79	133.3	5.26
39. low ^{3}He + ^{3}He rate	1.815	.02028	.2761	.2426	.7135	.00138	.00090	.01735	4	.00008	.00049	24.22	8.09	135.2	5.48
40. high $p + {}^{14}$N rate	1.816	.02029	.2762	.2426	.7134	.00133	.00084	.01616	4	.00008	.00168	24.30	8.15	136.4	5.36
41. low $p + {}^{14}$N rate	1.813	.02029	.2758	.2425	.7137	.00149	.00102	.01993	4	.00024	.00238	24.24	7.78	131.7	5.35
42. high $p + {}^{7}$Be rate	1.814	.02030	.2760	.2424	.7136	.00140	.00091	.01771	4	.00001	.00004	24.36	8.50	135.2	5.89
43. low $p + {}^{7}$Be rate	1.814	.02030	.2760	.2424	.7136	.00140	.00091	.01772	4	.00001	.00004	24.36	7.26	132.5	4.77
44. high $p + {}^{7}$Li rate	1.814	.02030	.2760	.2424	.7136	.00140	.00091	.01771	4	.00001	.00006	38.07	7.89	133.8	5.33

Table 1—Continued

Solar Model	α	Z_0	Y_0	Y_e	R_{ce} ($R_\odot$)	rms $\delta c/c$ for: all-r	rms $\delta c/c$ for: < 0.6	rms $\delta\rho/\rho$	relative rms vs.	relative rms $\Delta c/c$	relative rms $\Delta\rho/\rho$	$f_{\rm Li}$	$\Phi_{\rm Cl}$	$\Phi_{\rm Ga}$	$\Phi_{\rm B}$
45. low $p+{}^7$Li rate	1.814	.02030	.2760	.2424	.7136	.00139	.00091	.01772	4	.00001	.00005	15.69	7.89	133.8	5.33
46. CF88 nuclear rates	1.832	.02018	.2767	.2440	.7117	.00077	.00035	.00500	4	.00090	.01709	16.28	7.85	130.4	5.46
47. 20% low $D_{\rm He}$	1.781	.02018	.2760	.2485	.7169	.00217	.00162	.02439	4	.00084	.00682	20.15	7.71	132.9	5.20
48. 20% high $D_{\rm He}$	1.846	.02038	.2760	.2368	.7106	.00080	.00046	.01171	4	.00081	.00635	29.03	8.12	135.2	5.51
49. 40% low D_Z	1.824	.01949	.2725	.2385	.7128	.00165	.00130	.02187	4	.00038	.00420	18.43	7.42	131.2	4.98
50. 40% high D_Z	1.804	.02110	.2795	.2463	.7145	.00129	.00059	.01412	4	.00033	.00369	32.46	8.42	136.9	5.72

[a] Mixing length parameter α, pre-solar metallicity Z_0 and helium mass fraction Y_0, present envelope helium abundance Y_e, position R_{ce} of the base of envelope convection, rms fractional sound speed and density differences relative to the Sun's inferred helioseismic profiles and relative to the reference standard solar model, pre-main-sequence lithium depletion factor $f_{\rm Li}$, predicted capture rates (in SNU) $\Phi_{\rm Cl}$ and $\Phi_{\rm Ga}$ for chlorine and gallium experiments, respectively, and predicted flux $\Phi_{\rm B}$ of ^{8}B neutrinos (in units of 10^6 cm s^{-1}).

[b] Reference standard solar model: OPAL EOS at $\log\rho \gtrsim -1.5$, MHD EOS at $\log\rho \lesssim -2$, high-T opacities $\kappa_{\rm OPAL:GN93}$ interpolated in $Z_\kappa = Z_h \equiv Z_0\,[\sum_{heavy} X_i]/[\sum_{heavy}(X_i)_0]$ as well as in "excess" C and O (such that $C_{ex} + O_{ex} \equiv CO_{ex} = Z - Z_\kappa$), low-T opacities $\kappa_{\rm Alexander}$, NACRE nuclear rates, gravitational settling of He and heavy elements, $Z/X = 0.0245$, $L_\odot = 3.854\times10^{33}$ erg s^{-1}, $R_\odot = 695.98$ Mm, and $t_\odot = 4.6$ Gyr; both fine-zoned and coarse-zoned cases were computed. Variant models have the same input values, except as specified in the first column.

[c] OPALeos-midT: use OPAL EOS at $\log T \gtrsim 4.0$, MHD EOS at $\log T \lesssim 3.9$.

[d] OPALeos-lowT: use OPAL EOS at $\log T \gtrsim 3.75$, MHD EOS at $\log T \lesssim 3.7$ (on the main sequence, MHD EOS is only used outside the photosphere).

[e] This reference standard solar model and all subsequent models in the table use the coarse zoning.

[f] For these cases, the relative rms values compare the coarse-zoned cases to the corresponding fine-zoned cases.

[g] For these cases, the relative rms values compare the variant models with the case relative to which the parameter variation was performed.

[h] Most recent solar luminosity value of $L_\odot = L_{best} \equiv 3.842\times10^{33}$ erg s^{-1}.

[i] OPAL opacities not interpolated in "excess" C and O, i.e., opacities computed as if the CNO element abundance profiles in the Sun were always in the same proportion to the Fe profile ($Z_k = Z_h \neq Z$, but no correction term: $CO_{ex} = 0.0$).

[j] "Unmatched κ" means that Z/X has been varied relative to the recommended value of the given mixture (for which the OPAL opacities had been computed).

Table 2. Helioseismically Measured Present Solar Envelope Helium Abundance Y_e

Y_e Using OPAL Eos	Y_e Using MHD Eos	Reference
...	0.242 ± 0.003	1
0.249 ± 0.001	≈ 0.25	2
≈ 0.23[a]	≈ 0.25[a]	3
0.248 ± 0.001	0.232 ± 0.006	4
0.248 ± 0.001	≈ 0.252	5
0.248 ± 0.002	≈ 0.242	6
≈ 0.226[b]	...	7
0.2539 ± 0.0005	0.2457 ± 0.0005	8

[a] Obtained via an entropy calibration.

[b] Obtained from a fit to a solar sound speed profile, not a direct helioseismic inversion.

References. — (1) Pérez Hernández & Christensen-Dalsgaard 1994, (2) Basu & Antia 1995, (3) Baturin & Ayukov 1997, (4) Kosovichev 1997, (5) Basu 1998, (6) Richard et al. 1998, (7) Shibahashi et al. 1999, (8) Di Mauro et al. 2002